

Resonant States in the Shell Model

A. I. Mazur^a, A. M. Shirokov^{a,b,c}, I. A. Mazur^a and J. P. Vary^c

^a*Department of Physics, Pacific National University, Khabarovsk 680035, Russia*

^b*Skobeltsyn Institute of Nuclear Physics, Lomonosov Moscow State University, Moscow 119991, Russia*

^c*Department of Physics and Astronomy, Iowa State University, Ames, Iowa 50011, USA*

Abstract

We suggest a method for calculating scattering phase shifts and energies and widths of resonances which utilizes only eigenenergies obtained in variational calculations with oscillator basis and their dependence on oscillator basis spacing $\hbar\Omega$. We make use of simple expressions for the S -matrix at eigenstates of a finite (truncated) Hamiltonian matrix in the oscillator basis obtained in the HORSE (J -matrix) formalism of quantum scattering theory. The validity of the suggested approach is verified in calculations with model Woods–Saxon potentials and applied to calculations of $n\alpha$ resonances and non-resonant scattering using the no-core shell model.

Keywords: *No-core shell model; HORSE (J -matrix) formalism of quantum scattering theory; resonance energy and width; S -matrix poles*

1 Introduction

To calculate energies of nuclear ground states and other bound states within various shell model approaches, one conventionally starts by calculating the $\hbar\Omega$ -dependence of the energy $E_\nu(\hbar\Omega)$ of the bound state ν in some model space. The minimum of $E_\nu(\hbar\Omega)$ is correlated with the energy of the state ν . The convergence of calculations and accuracy of the energy prediction is estimated by comparing with the results obtained in neighboring model spaces. To improve the accuracy of theoretical predictions, various extrapolation techniques have been suggested recently [1–13] which make it possible to estimate the binding energies in the complete infinite shell-model basis space. The studies of extrapolations to the infinite model spaces reveal general trends of convergence patterns of shell model calculations.

Is it possible to study nuclear states in the continuum, low-energy scattering and resonant states in particular, in the shell model using bound state techniques? A conventional belief is that the energies of shell-model states in the continuum should be associated with the resonance energies. It was shown however in Ref. [14, 15] that the energies of shell-model states may appear well above the energies of resonant states, especially for broad resonances. Moreover, the analysis of Refs. [14, 15] clearly demonstrated that the shell model should also generate some states in a non-resonant nuclear continuum. The nuclear resonance properties can be studied in the Gamow shell model, including the *ab initio* no-core Gamow shell model (NCGSM) [16, 17]. Another option is to combine the shell model with resonating group method (RGM). An impressive progress in the description of various nuclear reactions was achieved by means of the combined no-core shell model/RGM (NCSM/RGM) approach [18–23].

Proceedings of the International Conference ‘Nuclear Theory in the Supercomputing Era — 2014’ (NTSE-2014), Khabarovsk, Russia, June 23–27, 2014. Eds. A. M. Shirokov and A. I. Mazur. Pacific National University, Khabarovsk, Russia, 2016, p. 183.

<http://www.ntse-2014.khb.ru/Proc/A.Mazur.pdf>.

Both NCGSM and NCSM/RGM complicate essentially the shell model calculations. Is it possible to get some information about unbound nuclear states directly from the results of calculations in NCSM or in other versions of the nuclear shell model without introducing additional Berggren basis states as in NCGSM or additional RGM calculations as in the NCSM/RGM approach?

The general behaviour of shell model eigenstates at positive energies (or just at the energies above various thresholds) is not well-studied and there is no well-established extrapolation technique to the infinite basis space for resonances. Generally, a complete study of the nuclear continuum can be performed by extending the nuclear shell model with the J -matrix formalism of scattering theory. The J -matrix formalism has been suggested in atomic physics [24, 25]. Later it was independently rediscovered in nuclear physics [26, 27] and was successfully used in shell-model applications [28]. The J -matrix approach utilizes diagonalization of the Hamiltonian in one of two bases: the so-called Laguerre basis that is of a particular interest for atomic physics applications and the oscillator basis that is appropriate for nuclear physics. The version of the J -matrix formalism with the oscillator basis is also sometimes referred to as an Algebraic Version of RGM [26] or as a HORSE (Harmonic Oscillator Representation of Scattering Equations) method [29] — we shall use the latter nomenclature in what follows.

We note that a direct implementation of the HORSE formalism in modern large-scale shell-model calculations is very complicated and unpractical: the HORSE method requires calculation of a huge number of eigenstates while modern shell-model codes usually utilize the Lanczos algorithm which provides only the few lowest Hamiltonian eigenstates. Furthermore, the HORSE method needs also the weight of the highest component of the wave function of each eigenstate which is usually obtained with a low precision. On the other hand, the HORSE formalism can be used for a simple calculation of the scattering phase shift or S -matrix at a single energy $E_\nu(\hbar\Omega)$ which is an eigenstate of the shell-model Hamiltonian. In this case, the HORSE phase shift calculation requires only the value of the energy $E_\nu(\hbar\Omega)$ and the basis parameters (the $\hbar\Omega$ value and the basis truncation). We shall refer to such a simplified approach as a Single State HORSE (SS-HORSE) method. Varying the shell-model parameter $\hbar\Omega$ and using results from a set of basis spaces, we generate a variation of $E_\nu(\hbar\Omega)$ in some energy range and hence we can calculate the phase shifts in that energy range.

Calculations of scattering phase shifts at the eigenenergies of the Hamiltonian in the oscillator basis and obtaining the phase shift energy dependence by variation of basis parameters, was recently performed in Ref. [5] using another (not the HORSE) technique. A detailed study of scattering phase shifts at eigenenergies of the Hamiltonian in arbitrary finite \mathcal{L}^2 basis was performed in Ref. [30]. This study was based on the theory of spectral shift functions introduced by I. M. Lifshitz nearly 70 years ago [31] and later forgotten by physicists though used up to now by mathematicians (see Ref. [30] and references therein).

Another method to obtain scattering phase shifts from bound state calculations in a harmonic oscillator basis features the use of an additional harmonic oscillator potential [32]. The method was demonstrated with nucleon-nucleon scattering where it reveals a challenge of needing a large basis to access the low-energy scattering region.

It is worth noting here that approximate resonant widths can be extracted from bound state approaches to many-body nuclear systems using a relation between the partial width in a specified breakup channel and an integral over the “interaction region” where all of the nucleons are close to each other. This method was described in detail in Ref. [33] where it was used to evaluate widths of resonances in light nuclei based on the variational Monte Carlo calculations. It has been used before in combination with other many-body approaches (see Ref. [33] for the list of respective

references), in particular, it can be utilized within the nuclear shell model. However this approach is applicable to narrow enough resonances only and is unable to provide information about non-resonant scattering.

In this contribution, we suggest a simpler and more powerful approach. We formulate below a method for calculating low-energy phase shifts and for extracting resonant energies E_r and widths Γ from the shell model results, or, generally, from results of any variational calculation with a finite oscillator basis. We apply the SS-HORSE formalism to calculate the S -matrix in the energy interval of variation of one of the Hamiltonian eigenenergies $E_\nu(\hbar\Omega)$ due to variation of $\hbar\Omega$ and truncation boundary of the Hamiltonian matrix. We use either a low-energy expansion of the S -matrix or express the S -matrix as a pole term plus slowly varying with energy background terms and fit the expansion parameters to describe the S -matrix behaviour in the above energy interval. The low-energy phase shifts δ_ℓ , the resonant energy E_r and width Γ appear as a result of this fit. We obtain relations describing the general behaviour of shell-model states associated with a resonance or with a non-resonant continuum as functions of $\hbar\Omega$ and truncation boundary of the Hamiltonian matrix. This approach is tested in calculations of phase shifts and resonance parameters of two-body scattering with model potential. Next we apply the SS-HORSE method to the calculation of resonances and of non-resonant continuum in the neutron- α scattering based on No-core Shell Model (NCSM) results obtained with the JISP16 NN interaction [34, 35]. This paper elaborates on the work presented in Refs. [36, 37].

In our earlier study [38], we evaluated resonant energies E_r and widths Γ using the SS-HORSE and Breit–Wigner formula for the description of resonances. The Breit–Wigner formula describes the phase shifts and S -matrix only in the case of narrow resonances and only in a narrow energy interval in the vicinity of the resonance. As a result, the approach of Ref. [38] can be used only in rare cases when the eigenenergies of the truncated Hamiltonian are obtained very close to the resonant energy E_r and cannot provide an accurate description of resonant parameters even in these rare cases. This drawback is eliminated in the current study.

The paper is organized as follows. We present in Section 2 the basic relations of the HORSE formalism, derive the SS-HORSE method and present all equations needed to calculate phase shifts, S -matrix and resonant parameters E_r and Γ . The SS-HORSE approach to the calculation of resonant energy and width is verified in Section 3 using a two-body scattering with a model potential. Section 4 is devoted to calculations of resonances in $n\alpha$ scattering based on NCSM calculations of ${}^5\text{He}$ with JISP16 NN interaction. Conclusions are presented in Section 5.

2 SS-HORSE approach to calculation of low-energy scattering and resonant parameters

2.1 HORSE formalism

The J -matrix approach and HORSE in particular are widely used in various applications. Some of the recent applications together with pioneering papers where the J -matrix has been suggested, can be found in the book [39]. We sketch here the basic relations and ideas of the HORSE formalism for the two-body single-channel scattering following our papers [29, 40, 41].

The radial wave function $u_\ell(k, r)$ describing the relative motion in the partial wave with orbital momentum ℓ is expanded within the HORSE formalism in an infinite series of radial oscillator functions $R_{N\ell}(r)$,

$$u_\ell(k, r) = \sum_{N=N_0, N_0+2, \dots, \infty} a_{N\ell}(k) R_{N\ell}(r), \quad (1)$$

where

$$R_{N\ell}(r) = (-1)^{(N-\ell)/2} \sqrt{\frac{2\Gamma(N/2 - \ell/2 + 1)}{r_0\Gamma(N/2 + \ell/2 + 3/2)}} \left(\frac{r}{r_0}\right)^{\ell+1} \exp\left(-\frac{r^2}{2r_0^2}\right) L_{(N-\ell)/2}^{\ell+\frac{1}{2}}\left(\frac{r^2}{r_0^2}\right). \quad (2)$$

Here k is the relative motion momentum, $L_n^\alpha(z)$ are associated Laguerre polynomials, the oscillator radius $r_0 = \sqrt{\frac{\hbar}{m\Omega}}$, m is the reduced mass of colliding particles, $\hbar\Omega$ is the oscillator level spacing, $N = 2n + \ell$ is the oscillator quanta while n is the oscillator principal quantum number, the minimal value of oscillator quanta $N_0 = \ell$. Using the expansion (1) we transform the radial Schrödinger equation

$$H^\ell u_\ell(k, r) = E u_\ell(k, r) \quad (3)$$

into an infinite set of linear algebraic equations,

$$\sum_{N'=N_0, N_0+2, \dots, \infty} (H_{NN'}^\ell - \delta_{NN'} E) a_{N'\ell}(k) = 0, \quad N = N_0, N_0 + 2, \dots, \quad (4)$$

where $H_{NN'}^\ell = T_{NN'}^\ell + V_{NN'}^\ell$ are matrix elements of the Hamiltonian H^ℓ in the oscillator basis, and $T_{NN'}^\ell$ and $V_{NN'}^\ell$ are kinetic and potential energy matrix elements respectively.

The kinetic energy matrix elements $T_{NN'}^\ell$ are known to form a tridiagonal matrix, i. e., the only non-zero matrix elements are

$$\begin{aligned} T_{NN}^\ell &= \frac{1}{2} \hbar\Omega(N + 3/2), \\ T_{N, N+2}^\ell &= T_{N+2, N}^\ell = -\frac{1}{4} \hbar\Omega \sqrt{(N - \ell + 2)(N + \ell + 3)}. \end{aligned} \quad (5)$$

These matrix elements are seen to increase linearly with N for large N . On the other hand, the potential energy matrix elements $V_{NN'}^\ell$ decrease as $N, N' \rightarrow \infty$. Hence the kinetic energy dominates in the Hamiltonian matrix at large enough N and/or N' . Therefore a reasonable approximation is to truncate the potential energy matrix at large N and/or N' , i. e., to approximate the interaction V by a nonlocal separable potential \tilde{V} of the rank $\mathbb{N} = (\mathbb{N} - N_0)/2 + 1$ with matrix elements

$$\tilde{V}_{NN'}^\ell = \begin{cases} V_{NN'}^\ell & \text{if } N \leq \mathbb{N} \text{ and } N' \leq \mathbb{N}; \\ 0 & \text{if } N > \mathbb{N} \text{ or } N' > \mathbb{N}. \end{cases} \quad (6)$$

The approximation (6) is the only approximation within the HORSE method; for the separable interaction of the type (6), the HORSE formalism suggests exact solutions. Note, the kinetic energy matrix is not truncated within the HORSE theory contrary to conventional variational approaches like the shell model. Hence the HORSE formalism suggests a natural generalization of the shell model.

The complete infinite harmonic oscillator basis space can be divided into two subspaces according to truncation (6): an internal subspace spanned by oscillator functions with $N \leq \mathbb{N}$ where the interaction V is accounted for and an asymptotic subspace spanned by oscillator functions with $N > \mathbb{N}$ associated with the free motion.

Algebraic equations (4) in the asymptotic subspace take the form of a second order finite-difference equation:

$$T_{N, N-2}^\ell a_{N-2, \ell}^{ass}(E) + (T_{NN}^\ell - E) a_{N\ell}^{ass}(E) + T_{N, N+2}^\ell a_{N+2, \ell}^{ass}(E) = 0. \quad (7)$$

Any solution $a_{N\ell}^{ass}(E)$ of Eq. (7) can be expressed as a superposition of regular $S_{N\ell}(E)$ and irregular $C_{N\ell}(E)$ solutions,

$$a_{N\ell}^{ass}(E) = \cos \delta_\ell S_{N\ell}(E) + \sin \delta_\ell C_{N\ell}(E), \quad N \geq \mathbb{N}, \quad (8)$$

where δ_ℓ is the scattering phase shift. The solutions $S_{N\ell}(E)$ and $C_{N\ell}(E)$ have simple analytical expressions [25, 27, 29, 40]:

$$S_{N\ell}(E) = \sqrt{\frac{\pi\Gamma(N/2 - \ell/2 + 1)}{\Gamma(N/2 + \ell/2 + 3/2)}} q^{\ell+1} \exp\left(-\frac{q^2}{2}\right) L_{(N-\ell)/2}^{\ell+1/2}(q^2), \quad (9)$$

$$C_{N\ell}(E) = (-1)^\ell \sqrt{\frac{\pi\Gamma(N/2 - \ell/2 + 1)}{\Gamma(N/2 + \ell/2 + 3/2)}} \frac{q^{-\ell}}{\Gamma(-\ell + 1/2)} \times \exp\left(-\frac{q^2}{2}\right) \Phi(-N/2 - \ell/2 - 1/2, -\ell + 1/2; q^2), \quad (10)$$

where $\Phi(a, b; z)$ is a confluent hypergeometric function and q is a dimensionless momentum,

$$q = \sqrt{\frac{2E}{\hbar\Omega}}. \quad (11)$$

The solutions $a_{N\ell}(E)$ of the algebraic set (4) in the internal subspace $N \leq \mathbb{N}$ are expressed through the solutions $a_{N\ell}^{ass}(E)$ in the asymptotic subspace $N \geq \mathbb{N}$:

$$a_{N\ell}(E) = \mathcal{G}_{N\mathbb{N}}(E) T_{\mathbb{N}, \mathbb{N}+2}^\ell a_{\mathbb{N}+2, \ell}^{ass}(E), \quad N = N_0, N_0 + 2, \dots, \mathbb{N}. \quad (12)$$

Here the matrix elements

$$\mathcal{G}_{NN'}(E) = - \sum_{\nu=0}^{\mathcal{N}-1} \frac{\langle N\ell|\nu\rangle\langle\nu|N'\ell\rangle}{E_\nu - E} \quad (13)$$

are related to the Green's function of the Hamiltonian $H^{\mathbb{N}}$ which is the Hamiltonian H^ℓ truncated to the internal subspace, and are expressed through eigenenergies E_ν , $\nu = 0, 1, 2, \dots, \mathcal{N} - 1$ (\mathcal{N} is the dimensionality of the basis) and respective eigenvectors $\langle N\ell|\nu\rangle$ of the Hamiltonian $H^{\mathbb{N}}$:

$$\sum_{N'=N_0, N_0+2, \dots, \mathbb{N}} H_{NN'}^\ell \langle N'\ell|\nu\rangle = E_\nu \langle N\ell|\nu\rangle, \quad N = N_0, N_0 + 2, \dots, \mathbb{N}. \quad (14)$$

A relation for calculation of the scattering phase shifts δ_ℓ can be obtained through the matching condition

$$a_{N\ell}(E) = a_{N\ell}^{ass}(E). \quad (15)$$

Using Eqs. (8), (12) and (15) it is easy to obtain [25, 27, 29, 40]

$$\tan \delta_\ell(E) = - \frac{S_{N\ell}(E) - \mathcal{G}_{N\mathbb{N}}(E) T_{\mathbb{N}, \mathbb{N}+2}^\ell S_{\mathbb{N}+2, \ell}(E)}{C_{N\ell}(E) - \mathcal{G}_{N\mathbb{N}}(E) T_{\mathbb{N}, \mathbb{N}+2}^\ell C_{\mathbb{N}+2, \ell}(E)}. \quad (16)$$

The respective expression for the S -matrix reads

$$S(E) = \frac{C_{N\ell}^{(-)}(E) - \mathcal{G}_{N\mathbb{N}}(E) T_{\mathbb{N}, \mathbb{N}+2}^\ell C_{\mathbb{N}+2, \ell}^{(-)}(E)}{C_{N\ell}^{(+)}(E) - \mathcal{G}_{N\mathbb{N}}(E) T_{\mathbb{N}, \mathbb{N}+2}^\ell C_{\mathbb{N}+2, \ell}^{(+)}(E)}, \quad (17)$$

where

$$C_{N\ell}^{(\pm)}(E) = C_{N\ell}(E) \pm S_{N\ell}(E). \quad (18)$$

We are using here the single-channel version of the HORSE formalism described above. The multi-channel HORSE formalism is discussed in detail in Refs. [25, 29, 40].

2.2 SS-HORSE method

A direct HORSE extension of modern large-scale shell-model calculations is unpractical. Note, Eq. (13) involves a sum over all shell-model eigenstates of a given spin-parity, i. e., over millions or even billions of states in modern NCSM applications. These states should be accurately separated from those having center-of-mass excitations. Unfortunately one cannot restrict the sum in Eq. (13) to some small enough set of eigenstates: even for the energies E close enough to one of the low-lying eigenstates E_ν , the contribution of some high-lying eigenstates to the sum in Eq. (13) can be essential: in model two-body problems describing, e. g., $n\alpha$ scattering, the growth of the denominator in the r.h.s. of Eq. (13) is compensated by the growth of the numerator; in NCSM calculations of ${}^5\text{He}$, the many-body eigenstates concentrate around the eigenstates of the model two-body Hamiltonian and though the contribution of each particular NCSM eigenstate is small, the sum of their contributions is large and close to the contribution of the respective state of the model Hamiltonian. A calculation of a large number of many-body eigenstates is too computationally expensive. Note, in many-body applications, one also needs to calculate the components $\langle N\ell|\nu\rangle$ of the wave function which should be projected on the scattering channel of interest; this projection requires numerous applications of Talmi–Moshinsky transformations which increase the computational cost and makes it very difficult to achieve a reasonable accuracy of the final sum in Eq. (13) due to computer noise.

To avoid these difficulties, we propose the SS-HORSE approach which requires calculations of the S -matrix or phase shifts only at $E = E_\nu$, i. e., at the energy equal to one of the lowest eigenstates lying above the reaction threshold. Equations (16) and (17) are essentially simplified in this case and reduce to

$$\tan \delta_\ell(E_\nu) = -\frac{S_{\mathbb{N}+2,\ell}(E_\nu)}{C_{\mathbb{N}+2,\ell}(E_\nu)} \quad (19)$$

and

$$S(E_\nu) = \frac{C_{\mathbb{N}+2,\ell}^{(-)}(E_\nu)}{C_{\mathbb{N}+2,\ell}^{(+)}(E_\nu)}. \quad (20)$$

Varying \mathbb{N} and $\hbar\Omega$ we obtain eigenvalues E_ν and hence phase shifts and S -matrix in some energy interval. An accurate parametrization of $\delta_\ell(E)$ and S -matrix in this energy interval makes it possible to extrapolate them to a larger energy interval and to calculate the resonance energy and width.

The use of Eqs. (19) and (20) drastically reduces the computational burden in many-body calculations. Within this SS-HORSE approach we need only one or probably very few low-lying eigenstates which energies should be calculated relative to the respective threshold, e. g., in the case of $n\alpha$ scattering we need to subtract from the ${}^5\text{He}$ energies the ${}^4\text{He}$ ground state energy. Another interesting and important feature of the SS-HORSE technique is that the Eqs. (19) and (20) do not involve any information regarding the eigenvectors $\langle N\ell|\nu\rangle$. This essentially simplifies calculations, the information about a particular channel under consideration is present only in the threshold energy used to calculate the eigenenergies E_ν and in the channel orbital momentum ℓ . Equations (19) and (20) establish some correlations between scattering in different channels when the channel coupling can be neglected, a topic that deserves further investigation but is outside the scope of the present work.

We use here Eqs. (19) and (20) to obtain phase shifts and S -matrix from Hamiltonian diagonalization results. However these equations can be used in inverse manner: if the phase shifts are known from analysis of experimental scattering data, one can solve Eq. (19) to obtain eigenenergies E_ν which the shell model Hamiltonian should have to be consistent with scattering data. The direct use of Eq. (19) essentially simplifies the inverse approach to nucleon-nucleus scattering suggested in Refs. [14, 15].

We see that the scattering phase shifts are determined by the universal function

$$f_{\mathbb{N}\ell}(E) = -\arctan\left[\frac{S_{\mathbb{N}+2,\ell}(E)}{C_{\mathbb{N}+2,\ell}(E)}\right]. \quad (21)$$

This is a smooth monotonically decreasing function which drops down by $n\pi$ as energy E varies from 0 to ∞ . At low energies when

$$E \ll \frac{1}{8}\hbar\Omega(\mathbb{N}+2-\ell)^2, \quad (22)$$

one can replace the functions $S_{\mathbb{N}+2,\ell}(E)$ and $C_{\mathbb{N}+2,\ell}(E)$ in Eq. (21) by their asymptotic expressions at large \mathbb{N} (see Ref. [40]) to obtain

$$f_{\mathbb{N}\ell}(E) \approx f_{\ell}^{l.e.}(E) = \arctan\left[\frac{j_{\ell}(2\sqrt{E/s})}{n_{\ell}(2\sqrt{E/s})}\right], \quad (23)$$

where

$$s = \frac{\hbar\Omega}{\mathbb{N}+7/2}, \quad (24)$$

and $j_l(x)$ and $n_l(x)$ are spherical Bessel and spherical Neumann functions. If additionally

$$E \gg \frac{1}{4}s = \frac{\hbar\Omega}{4(\mathbb{N}+7/2)}, \quad (25)$$

one can use asymptotic expressions for spherical Bessel and Neumann functions in Eq. (23) to get a very simple expression for the function $f_{\mathbb{N}\ell}(E)$:

$$f_{\mathbb{N}\ell}(E) \approx -2\sqrt{\frac{E}{s}} + \frac{\pi\ell}{2}. \quad (26)$$

The universal function $f_{\mathbb{N}\ell}(E)$ and its low-energy approximations (23) and (26) are shown in Fig. 1. The basis space in shell model applications is conventionally labeled by the maximal oscillator excitation quanta N_{\max} , and we use N_{\max} in Fig. 1 to distinguish functions $f_{\mathbb{N}\ell}(E)$ corresponding to different basis sizes. Obviously,

$$\mathbb{N} = N_{\max} + \ell \quad (27)$$

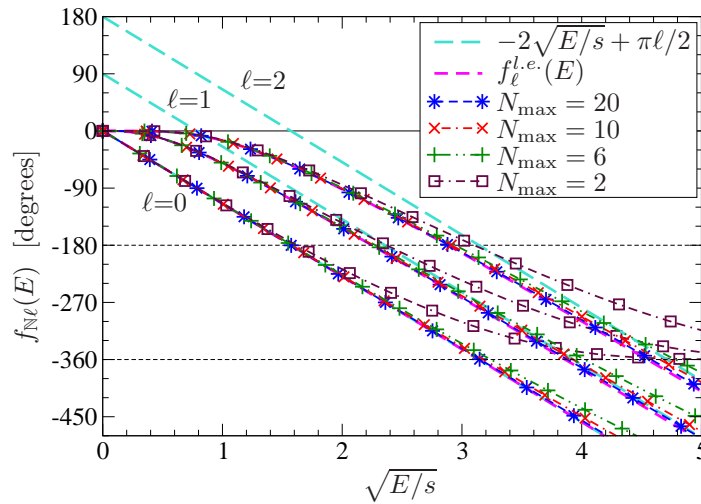


Figure 1: The function $f_{\mathbb{N}\ell}(E)$ (symbols) for different \mathbb{N} and ℓ and its low-energy approximations $f_{\ell}^{l.e.}(E)$ [see Eq. (23)] and $-2\sqrt{E/s} + \pi\ell/2$ [see Eq. (26)].

in the two-body scattering problem. The approximation (23) is seen to be very accurate at low energies even for small N_{\max} . This low-energy approximation, as expected, deviates from the function $f_{\mathbb{N}\ell}(E)$ as the energy E increases; the energy interval where the approximation (23) accurately describes $f_{\mathbb{N}\ell}(E)$ increases with \mathbb{N} or N_{\max} in accordance with inequality (22). In the case $\ell = 0$, the simple expression (26) is equivalent to the Eq. (23) and therefore describes the function $f_{\mathbb{N}\ell}(E)$ with the same accuracy. For $\ell > 0$ the simplified approximation (26) deviates from the approximation (23) and the function $f_{\mathbb{N}\ell}(E)$ at low energies, it can only be used in a relatively small energy interval defined by inequalities (22) and (25).

Due to Eq. (23), equation (19) at low energies can be reduced to

$$\tan \delta_\ell(E_\nu) = \frac{j_\ell(2\sqrt{E_\nu/s})}{n_\ell(2\sqrt{E_\nu/s})}. \quad (28)$$

This equation reveals the scaling at low energies: the oscillator basis parameters \mathbb{N} and $\hbar\Omega$ are not independent, they are entering equations relating the S -matrix and phase shifts with the eigenenergies of the Hamiltonian matrix in the oscillator basis not separately but only through the scaling variable s combining them in a particular manner. The scaling is useful within our approach for selecting eigenenergies E_ν obtained with different \mathbb{N} and $\hbar\Omega$ for the further analysis of phase shifts and S -matrix poles: the convergence of the results obtained by diagonalization of the Hamiltonian in oscillator basis is achieved within some interval of $\hbar\Omega$ values starting from some \mathbb{N} ; the converged results for E_ν should describe the same phase shifts with some accuracy, therefore, due to the scaling (28), these converged E_ν plotted as functions of the scaling parameter s should lie approximately on the same curve. By plotting E_ν vs s we can pick up for further analysis only those E_ν which form some curve as is illustrated later.

The scaling in variational oscillator-basis calculations of bound states was proposed in Refs. [2, 3]. We extend here the scaling property of the oscillator-basis calculations to the continuum states. We prefer to use the scaling parameter s in energy units rather than the scaling parameter λ_{sc} of Refs. [2, 3, 6, 13] in momentum units or the scaling parameter

$$L = \sqrt{2(\mathbb{N} + 7/2)} r_0 \quad (29)$$

in the units of length suggested in Ref. [5]. The parameter L includes a small correction to the scaling proposed in Refs. [2, 3] which was suggested in Ref. [5] based on numerical results. We obtain this correction automatically in our approach. Having this correction in mind, we get

$$s \sim \lambda_{sc}^2 \sim 1/L^2; \quad (30)$$

in other words, we propose generically the same scaling as discussed in Refs. [2–11, 13] but using another scaling parameter and extending the scaling to continuum states.

We derive the scaling property in a very different approach than that utilized in Refs. [2–5]. Therefore it is interesting to compare these scalings in more detail. One can analytically continue the Eqs. (19) and (20) to the complex energy or complex momentum plane, in particular, one can use these expressions at negative energies corresponding to bound states. Using asymptotic expressions of the functions $C_{\mathbb{N}+2,\ell}^{(+)}(E)$ and $C_{\mathbb{N}+2,\ell}^{(-)}(E)$ at large \mathbb{N} and negative energy E (see Ref. [40]), we obtain from Eq. (20):

$$S(E_\nu) = (-1)^\ell \exp\left(-4i\sqrt{\frac{E_\nu}{s}}\right), \quad E_\nu < 0. \quad (31)$$

On the other hand, the S -matrix $S(E_\nu)$ at negative energies E_ν in the vicinity of the pole associated with the bound state at energy $E_b < 0$ can be expressed as [42]

$$S(E_\nu) = \frac{D_\ell}{i\kappa_\nu - ik_b}, \quad (32)$$

where $E_\nu = -\frac{\hbar^2 \kappa_\nu^2}{2m}$, $E_b = -\frac{\hbar^2 k_b^2}{2m}$, momenta κ_ν and k_b are supposed to be positive, and D_ℓ can be expressed through the asymptotic normalization constant A_ℓ [42]:

$$D_\ell = (-1)^{\ell+1} i |A_\ell|^2. \quad (33)$$

Combining Eqs. (31)–(33), we obtain:

$$\kappa_\nu - k_b = -|A_\ell|^2 \exp\left(-\frac{4\kappa_\nu \hbar}{\sqrt{2ms}}\right). \quad (34)$$

This expression can be used for extrapolating the eigenenergies E_ν (or respective momenta κ_ν) obtained in a finite oscillator basis to the infinite basis space supposing that $E_\nu \rightarrow E_b$ as $\mathbb{N} \rightarrow \infty$.

The respective expression for extrapolating the oscillator basis eigenenergies derived in Refs. [2–5] rewritten in our notations, takes the form:

$$E_\nu - E_b = C_\ell \exp\left(-\frac{4k_b \hbar}{\sqrt{2ms}}\right). \quad (35)$$

There is some similarity, however there is also an essential difference between Eqs. (34) and (35). Both equations have similar exponents in the right-hand-side, however the exponent in our Eq. (34) involves momentum κ_ν associated with the eigenenergy E_ν while Eq. (35) involves momentum k_b associated with the converged energy E_b in the limit $\mathbb{N} \rightarrow \infty$. In the vicinity of the S -matrix pole [see Eq. (32)] κ_ν should not differ much from k_b ; we note however that k_b is conventionally treated as an additional fitting parameter (see Refs. [2–11]), i. e., it is supposed that $E_b \neq -\frac{\hbar^2 k_b^2}{2m}$, and hence there may be an essential difference between κ_ν and k_b in applications. Even more important is that the exponent in the right-hand-side controls the difference between the energies E_ν and E_b in Eq. (35) while in our Eq. (34) the exponent controls the difference between the momenta $\kappa_\nu \sim \sqrt{|E_\nu|}$ and $k_b \sim \sqrt{|E_b|}$. We plan to examine in detail in a separate publication which of the Eqs. (34) and (35) describes better the results of diagonalizations of realistic Hamiltonians in the oscillator basis for negative eigenenergies E_ν and which of them is more accurate in extrapolating the results for bound states obtained in finite oscillator bases to the infinite basis space.

Equations (19) and (20) can be used to obtain the phase shifts and S -matrix in some range of energies covered by eigenenergies E_ν obtained with various \mathbb{N} and $\hbar\Omega$. To interpolate the energy dependences of the phase shifts and S -matrix within and to extrapolate them outside this interval, we need accurate formulas for the phase shifts and S -matrix as functions of energy which we discuss in the next subsection.

2.3 Phase shifts and S -matrix at low energies

The scattering S -matrix as a function of the complex momentum k is known [42, 43] to have the following symmetry properties:

$$S(-k) = \frac{1}{S(k)}, \quad S(k^*) = \frac{1}{S^*(k)}, \quad S(-k^*) = S^*(k), \quad (36)$$

where star is used to denote the complex conjugation. The S -matrix can have poles either in the lower part of the complex momentum plane or on the imaginary momentum axis [42, 43]. The poles in the lower part of the complex momentum plane

at $k = \kappa_r \equiv k_r - i\gamma_r$ ($k_r, \gamma_r > 0$) due to the symmetry relations (36) are accompanied by the poles at $k = -\kappa_r^* \equiv -k_r - i\gamma_r$ and are associated with resonances at the energy

$$E_r = \frac{\hbar^2}{2m}(k_r^2 - \gamma_r^2) \quad (37)$$

and with the width

$$\Gamma = \frac{2\hbar^2}{m}k_r\gamma_r. \quad (38)$$

Bound states at energy $E_b = -\hbar^2k_b^2/2m$ are in correspondence with the poles on the positive imaginary momentum axis at $k = ik_b$ ($k_b > 0$), however some positive imaginary momentum poles can appear to be the so-called false or redundant poles [42] which do not represent any bound state. The poles at negative imaginary momentum at $k = -ik_v$ ($k_v < 0$) are associated with virtual states at energy $E_v = \hbar^2k_v^2/2m$.

If the S -matrix has a pole close to the origin either in the lower part of the complex momentum plane or on the imaginary momentum axis, it can be expressed at low energies as

$$S(k) = \Theta(k) S_p(k), \quad (39)$$

where $\Theta(k)$ is a smooth function of k and the pole term $S_p(k)$ in the case of a bound state or false pole ($p = b$), virtual ($p = v$) or a resonant state ($p = r$) takes the form [43]:

$$S_b(k) = -\frac{k + ik_b}{k - ik_b}, \quad (40)$$

$$S_v(k) = -\frac{k - ik_v}{k + ik_v}, \quad (41)$$

$$S_r(k) = \frac{(k + \kappa_r)(k - \kappa_r^*)}{(k - \kappa_r)(k + \kappa_r^*)}. \quad (42)$$

The S -matrix is expressed through the phase shifts $\delta_\ell(k)$ as

$$S(k) = e^{2i\delta_\ell(k)}, \quad (43)$$

hence the respective phase shifts

$$\delta_\ell(k) = \phi(k) + \delta_p(k), \quad (44)$$

where the pole contribution $\delta_p(k)$ from the bound state takes the form

$$\delta_b(E) = \pi - \arctan \sqrt{\frac{E}{|E_b|}}, \quad (45)$$

where π appears due to the Levinson theorem [43]. The contributions from the false, virtual and resonant poles are

$$\delta_f(E) = -\arctan \sqrt{\frac{E}{|E_f|}}, \quad (46)$$

$$\delta_v(E) = \arctan \sqrt{\frac{E}{E_v}}, \quad (47)$$

$$\delta_r(E) = -\arctan \frac{a\sqrt{E}}{E - b^2}, \quad (48)$$

where the resonance energy E_r and width Γ can be expressed through the parameters a and b as

$$E_r = b^2 - a^2/2, \quad (49)$$

$$\Gamma = a\sqrt{4b^2 - a^2}. \quad (50)$$

Due to Eq. (43), the S -matrix symmetries (36) require the phase shift $\delta_\ell(E)$ to be an odd function of k and its expansion in Taylor series of $\sqrt{E} \sim k$ includes only odd powers of \sqrt{E} :

$$\delta_\ell(E) = c\sqrt{E} + d(\sqrt{E})^3 + \dots \quad (51)$$

More, since $\delta_\ell \sim k^{2\ell+1}$ in the limit $k \rightarrow 0$, $c = 0$ in the case of p -wave scattering, $c = d = 0$ in the case of d -wave scattering, etc.

In applications to the non-resonant $n\alpha$ scattering in the $\frac{1}{2}^+$ state ($\ell = 0$), we therefore are using the following parametrization of the phase shifts:

$$\delta_0(E) = \pi - \arctan \sqrt{\frac{E}{|E_b|}} + c\sqrt{E} + d(\sqrt{E})^3 + f(\sqrt{E})^5. \quad (52)$$

The bound state pole contribution here is associated with the so-called Pauli-forbidden state. There are resonances in the $n\alpha$ scattering in the $\frac{1}{2}^-$ and $\frac{3}{2}^-$ states ($\ell = 1$); hence we parametrize these phase shifts as

$$\delta_1(E) = -\arctan \frac{a\sqrt{E}}{E - b^2} - \frac{a}{b^2}\sqrt{E} + d(\sqrt{E})^3. \quad (53)$$

This form guarantees that $\delta_1 \sim k^3$ in the limit of $E \rightarrow 0$.

3 Model problem

To test our SS-HORSE technique, we calculate the phase shifts and resonant parameters of $n\alpha$ scattering in a two-body approach treating neutron and α as structureless particles whose interaction is described by a Woods–Saxon type potential WSB

$$V_{n\alpha} = \frac{V_0}{1 + \exp[(r - R_0)/\alpha_0]} + (\mathbf{l} \cdot \mathbf{s}) \frac{1}{r} \frac{d}{dr} \frac{V_{ls}}{1 + \exp[(r - R_1)/\alpha_1]}, \quad (54)$$

with parameters fitted in Ref. [44]: $V_0 = -43$ MeV, $V_{ls} = -40$ MeV · fm², $R_0 = 2.0$ fm, $\alpha_0 = 0.70$ fm, $R_1 = 1.5$ fm, $\alpha_1 = 0.35$ fm. The matrix in the oscillator basis of the relative motion Hamiltonian with this interaction is diagonalized using $\hbar\Omega$ values ranging from 2.5 to 50 MeV in steps of 2.5 MeV and N_{\max} up to 20 for natural parity states $\frac{3}{2}^-$ and $\frac{1}{2}^-$ and up to 19 for unnatural parity states $\frac{1}{2}^+$.

3.1 Partial wave $\frac{3}{2}^-$

The lowest eigenstates E_0 obtained by diagonalization of the model Hamiltonian with the WSB potential are presented in Fig. 2 as a function of the scaling parameter s . It is seen that the eigenstates obtained with large enough N_{\max} values form a single curve in Fig. 2; however the eigenstates obtained with smaller N_{\max} start deviating from this curve at smaller $\hbar\Omega$ which correspond to smaller s values reflecting the convergence patterns of calculations in the finite oscillator basis. This feature is even more pronounced in the plot of the phase shifts obtained directly from eigenstates E_0

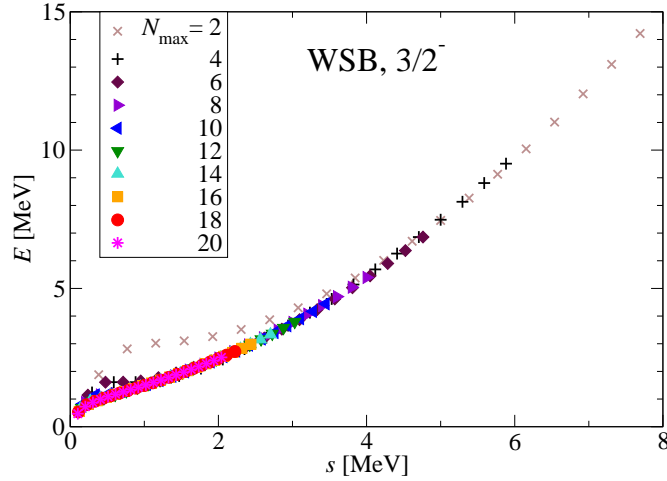


Figure 2: The lowest $\frac{3}{2}^-$ eigenstates E_0 of the model Hamiltonian with WSB potential obtained with various N_{\max} and $\hbar\Omega$ plotted as a function of the scaling parameter s .

using Eq. (19) (see Fig. 3). We need to exclude from the further SS-HORSE analysis the eigenstates deviating from the common curves in Figs. 2 and 3.

As we already mentioned, the scaling property of our SS-HORSE formalism has much in common with those proposed in Refs. [2, 3]. Using the nomenclature of Refs. [2, 3], we should use only eigenenergies E_0 which are not influenced by infra-red corrections. According to Refs. [2, 3], these eigenenergies are obtained with N_{\max} and $\hbar\Omega$ fitting inequality

$$\Lambda \equiv \sqrt{m\hbar\Omega(N_{\max} + \ell + 3/2)} > \Lambda_0, \quad (55)$$

where Λ_0 depends on the interaction between the particles. The value of $\Lambda_0 = 385 \text{ MeV}/c$ seems to be adequate for the potential WSB resulting in a reasonable selection of eigenenergies E_0 . The selection of eigenenergies according to this criterion is illustrated by the shaded area in Fig. 4 where we plot eigenenergies E_0 obtained with various N_{\max} as functions of $\hbar\Omega$. These selected eigenstates plotted as a function of the scaling parameter s in Fig. 5 and the respective SS-HORSE phase shifts in Fig. 6 are seen to produce smooth single curves.

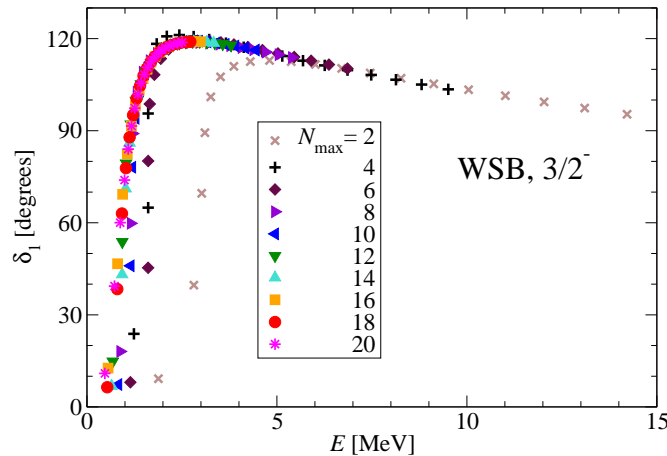


Figure 3: The $\frac{3}{2}^-$ phase shifts obtained directly from the WSB eigenstates E_0 using Eq. (19).

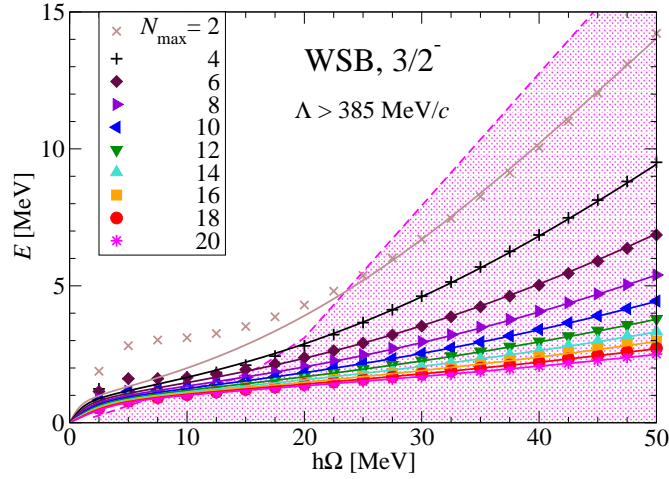


Figure 4: The lowest $\frac{3}{2}^-$ eigenenergies E_0 of the model WSB Hamiltonian obtained with various N_{\max} as functions of $\hbar\Omega$ and selection of eigenstates for the SS-HORSE analysis according to inequality $\Lambda > 385 \text{ MeV}/c$. The shaded area shows the selected E_0 values. Solid lines are solutions of Eq. (56) for energies E_0 with parameters a , b and d obtained by the fit.

The low-energy resonant $n\alpha$ scattering phase shifts in the $\frac{3}{2}^-$ state are described by Eq. (53). We need to fit the parameters a , b and d of this equation. Combining Eqs. (19), (27) and (53) we derive the following relation for resonant $n\alpha$ scattering in the $\frac{3}{2}^-$ state which can be also used for the $\frac{1}{2}^-$ state ($\ell = 1$ in both cases):

$$-\frac{S_{N_{\max}+3,1}(E_0)}{C_{N_{\max}+3,1}(E_0)} = \tan\left(-\arctan\frac{a\sqrt{E_0}}{E_0 - b^2} - \frac{a}{b^2}\sqrt{E_0} + d(\sqrt{E_0})^3\right). \quad (56)$$

We assign some values to the parameters a , b and d and solve this equation to find a set of E_0 values, $\mathcal{E}_0^{(i)} = E_0(N_{\max}^i, \hbar\Omega^i)$, $i = 1, 2, \dots, D$, for each combination

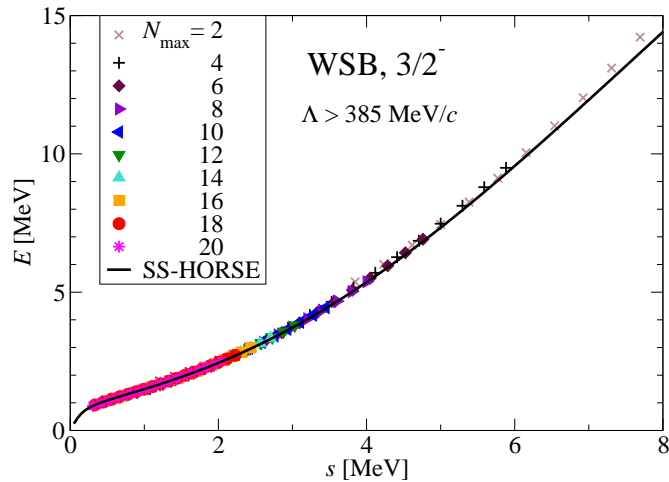


Figure 5: The $\frac{3}{2}^-$ WSB eigenstates E_0 selected according to $\Lambda > 385 \text{ MeV}/c$ plotted as a function of the scaling parameter s . The solid curve depicts solutions of Eq. (56) for energies E_0 with parameters a , b and d obtained by the fit with the respective selection of eigenstates.

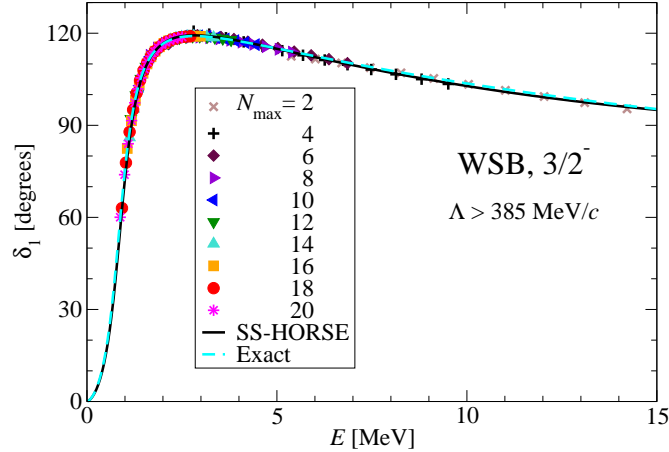


Figure 6: The $\frac{3}{2}^-$ WSB phase shifts obtained using Eq. (19) directly from eigenstates E_0 selected according to $\Lambda > 385$ MeV/ c (symbols). The solid curve depicts the phase shifts of Eq. (53) with parameters a , b and d obtained by the fit with the respective selection of eigenstates; the dashed curve is obtained by a numerical integration of the Schrödinger equation.

of N_{\max} and $\hbar\Omega$ [note, $\hbar\Omega$ enters definitions of functions $S_{N,\ell}(E)$ and $C_{N,\ell}(E)$, see Eqs. (9)–(11)]. The resulting set of $\mathcal{E}_0^{(i)}$ is compared with the set of selected eigenvalues $E_0^{(i)}$ obtained by the Hamiltonian diagonalization with respective N_{\max} and $\hbar\Omega$ values, and we minimize the rms deviation,

$$\Xi = \sqrt{\frac{1}{D} \sum_{i=1}^D \left(E_0^{(i)} - \mathcal{E}_0^{(i)} \right)^2}, \quad (57)$$

to find the optimal values of the parameters a , b and d . The obtained parameters are listed in the first row of Table 1. The resonance energy E_r and width Γ obtained by Eqs. (49) and (50) are also presented in Table 1. Note the accuracy of the fit: the rms deviation of 156 fitted energy eigenvalues is only 37 keV.

The behavior of E_0 as functions of $\hbar\Omega$ dictated by Eq. (56) with the fitted optimal parameters for various N_{\max} values is depicted by solid curves in Figs. 4 and 5. It is seen that these curves accurately describe the selected eigenvalues E_0 obtained by the Hamiltonian diagonalization. Note however a small deviation of the curve in Fig. 5 from the diagonalization results at large energies obtained with $N_{\max} = 2$ where the scaling become inaccurate, see Eq. (22). The phase shifts $\delta_1(E)$ obtained by Eq. (53) with fitted parameters are shown in the Fig. 6. It is seen that the SS-HORSE phase shifts are in excellent correspondence with the exact results obtained by numerical integration of the Schrödinger equation. The $\frac{3}{2}^-$ resonance energy and width are also well reproduced by our SS-HORSE technique (see Table 1).

In the above analysis we used oscillator bases with N_{\max} values up to $N_{\max} = 20$. Such large N_{\max} are accessible in two-body problems but are out of reach in modern many-body shell model applications. Therefore it is very important to check whether a reasonable accuracy of SS-HORSE phase shift and resonance parameter calculations can be achieved with significantly smaller N_{\max} .

We remove from the set of selected $\frac{3}{2}^-$ eigenstates $E_0^{(i)}$ those obtained with $N_{\max} > 6$ and use this new selection illustrated by Figs. 7 and 8 to calculate phase shifts and resonant parameters. All eigenenergies from this selection lie outside the resonance region as is seen in Fig. 9 where we plot the phase shifts as a function of energy. The SS-HORSE fit (see Table 1) nevertheless accurately reproduces the exact phase

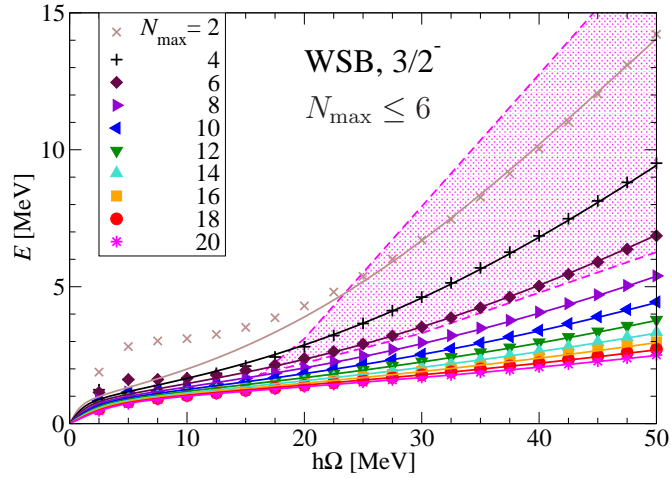


Figure 7: Selection of the lowest $\frac{3}{2}^-$ WSB eigenstates E_0 obtained with $N_{\max} \leq 6$. See Fig. 4 for details.

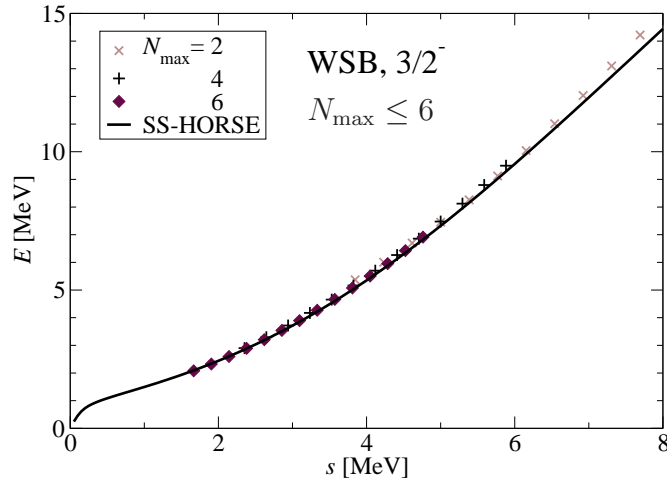


Figure 8: Selected lowest $\frac{3}{2}^-$ WSB eigenstates E_0 obtained with $N_{\max} \leq 6$ as a function of the scaling parameter s . See Fig. 5 for details.

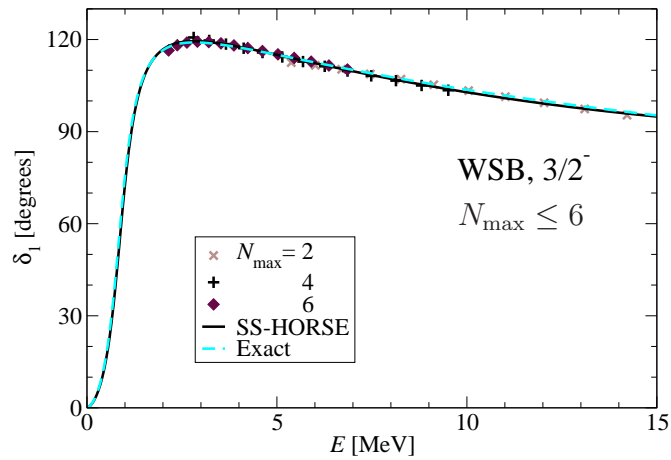


Figure 9: The $\frac{3}{2}^-$ WSB phase shifts generated by the selected eigenstates E_0 obtained with $N_{\max} \leq 6$. See Fig. 6 for details.

Table 1: $\frac{3}{2}^-$ resonance in $n\alpha$ scattering with model WSB potential: fitting parameters a , b , d of Eq. (56), resonance energy E_r and width Γ , rms deviation of fitted energies Ξ and the number of these fitted energies D for different selections of eigenvalues in comparison with exact results for E_r and Γ obtained by numerical location of the S -matrix pole. For the $N_{\max} \leq 6$ selection, Ξ and D for all energies from the previous selection are shown within brackets.

Selection	a (MeV $^{\frac{1}{2}}$)	b^2 (MeV)	$d \cdot 10^3$ (MeV $^{-\frac{3}{2}}$)	E_r (MeV)	Γ (MeV)	Ξ (keV)	D
$\Lambda > 385$ MeV/ c	0.412	0.948	5.41	0.863	0.785	37	156
$N_{\max} \leq 6$	0.411	0.948	5.30	0.863	0.782	70(38)	38(156)
Exact				0.836	0.780		

shifts (see Fig. 9) even in the resonance region and the $\frac{3}{2}^-$ resonance energy E_r and width Γ (see Table 1). To get such accuracy, it is very important to use the adequate phase shift parametrization (53) which guarantees the low-energy phase shift behaviour $\delta_\ell \sim k^{2\ell+1}$ and an accurate description of the resonance region by the pole term (48): our previous study [38] has clearly demonstrated that it is impossible to reproduce the resonant parameters and phase shifts in a wide enough energy interval without paying special attention to the low-energy phase shift description and by using the less accurate Breit–Wigner resonant phase shifts instead of the pole term (48) even when large N_{\max} eigenstates E_0 are utilized to say nothing about the selection of eigenstates obtained with small N_{\max} .

Solid lines in Figs. 4 and 7 present the eigenenergies E_0 for various N_{\max} values as functions of $\hbar\Omega$ obtained from the respective phase shift parametrization. It is seen that we accurately describe not only the eigenenergies from the shaded area utilized in the fit but also those corresponding to a wider range of $\hbar\Omega$ values. It is even more interesting that in the case of Fig. 7 where fitted are only the states with $N_{\max} \leq 6$, we also reproduce the eigenenergies obtained with much larger N_{\max} values with nearly the same rms deviation as in the case of the previous selection (see Table 1) when those larger N_{\max} eigenenergies were included in the fit. In other words, our SS-HORSE fit to the diagonalization results in small basis spaces makes it possible to ‘predict’ the diagonalization results obtained with much larger oscillator bases. This is very important for many-body shell-model applications and suggests a very efficient method of extrapolating the shell-model results in continuum to larger basis spaces.

3.2 Partial wave $\frac{1}{2}^-$

The lowest $\frac{1}{2}^-$ eigenstates of the model Hamiltonian with the WSB potential are shown as functions of $\hbar\Omega$ for various N_{\max} in Fig. 10 and as functions of the scaling parameter s in Fig. 11. All eigenenergies in this case seem to lie approximately on the same curve in Fig. 11; however the plot of the SS-HORSE phase shifts corresponding to these eigenstates (see Fig. 12) clearly indicates deviations from the common curve for eigenstates obtained with small N_{\max} values. We have already mentioned that the phase shifts are more sensitive to the convergence patterns and are somewhat more instructive for the selection of the eigenenergies.

As in the case of the $\frac{3}{2}^-$ partial wave, we start with the $\Lambda > 385$ MeV/ c selection of eigenenergies as is illustrated by Fig. 13 and by the shaded area in Fig. 10. The fitting method described in the previous subsection results in the parameters listed in the first row of Table 2. We obtain a reasonable fit with a small enough rms deviation of the 156 selected eigenenergies of 80 keV. The obtained phase shifts depicted in Fig. 14 are

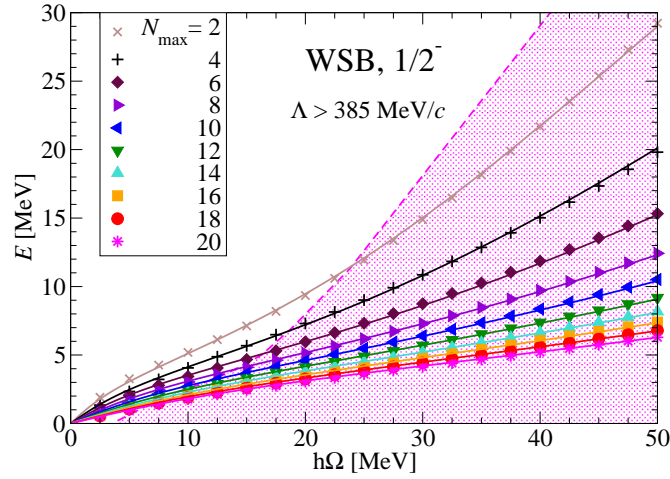


Figure 10: The lowest $\frac{1}{2}^-$ WSB eigenstates E_0 as functions of $\hbar\Omega$ and their $\Lambda > 385$ MeV/c selection. See Fig. 4 for details.

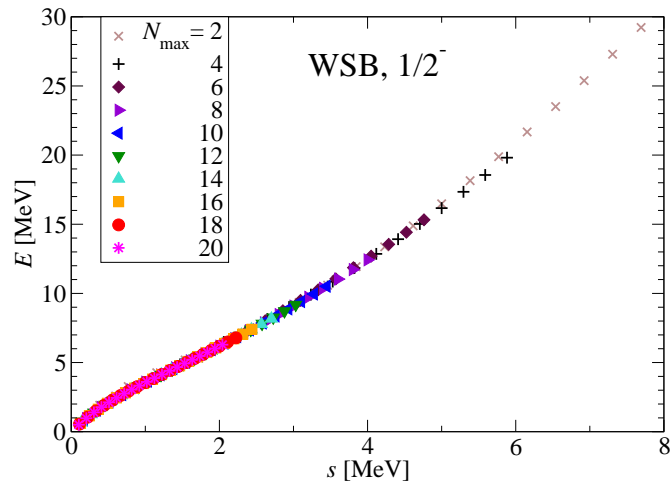


Figure 11: The lowest $\frac{1}{2}^-$ WSB eigenstates E_0 as a function of the scaling parameter s .

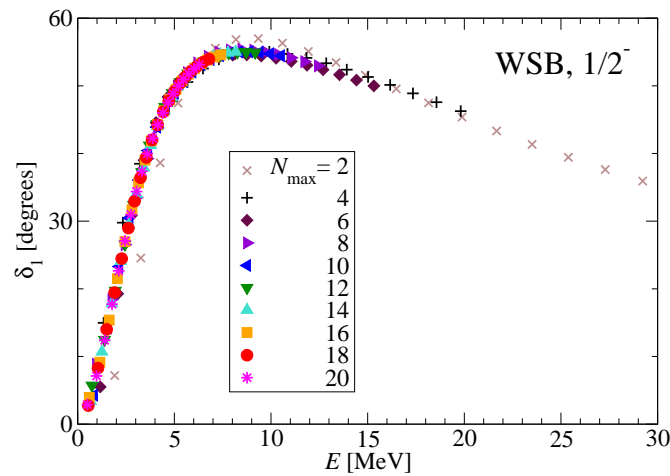


Figure 12: The $\frac{1}{2}^-$ phase shifts obtained directly from the WSB eigenstates E_0 using Eq. (19).

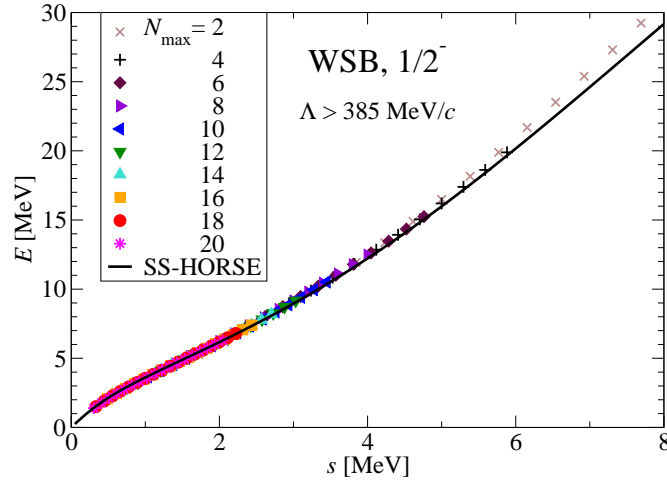


Figure 13: The $\Lambda > 385$ MeV/ c selected $\frac{1}{2}^-$ WSB eigenstates E_0 as a function of the scaling parameter s . See Fig. 5 for details.

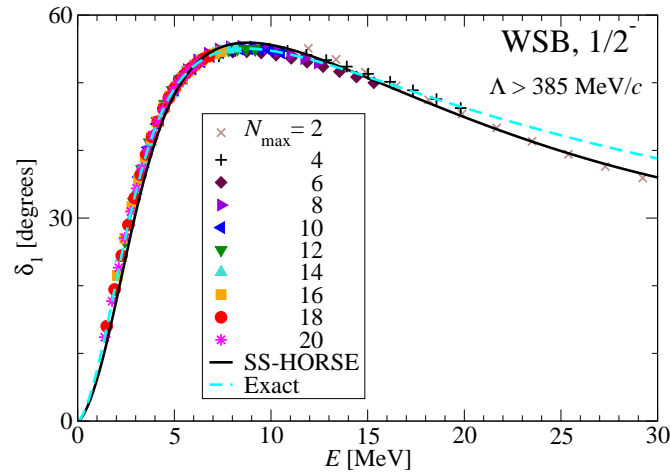


Figure 14: The $\frac{1}{2}^-$ WSB phase shifts generated by the $\Lambda > 385$ MeV/ c selected eigenstates E_0 . See Fig. 6 for details.

very close to the exact phases from numerical integration of the Schrödinger equation with the WSB potential up to the energy E of approximately 17 MeV. At higher energies we see some difference between the exact and SS-HORSE phases shifts which are completely governed in this energy region by the $N_{\max} = 2$ eigenenergies which are not expected to be close to convergence for the energy extrapolations and S -matrix description within the HORSE extension of the Hamiltonian. We note also

Table 2: Parameters of the $\frac{1}{2}^-$ WSB resonance. See Table 1 for details.

Selection	a (MeV $^{\frac{1}{2}}$)	b^2 (MeV)	$d \cdot 10^3$ (MeV $^{-\frac{3}{2}}$)	E_r (MeV)	Γ (MeV)	Ξ (keV)	D
$\Lambda > 385$ MeV/ c	1.780	3.636	3.18	2.05	6.00	80	156
$N_{\max} \leq 6$	1.822	3.818	2.77	2.16	6.30	75(84)	38(156)
Exact				1.66	5.58		

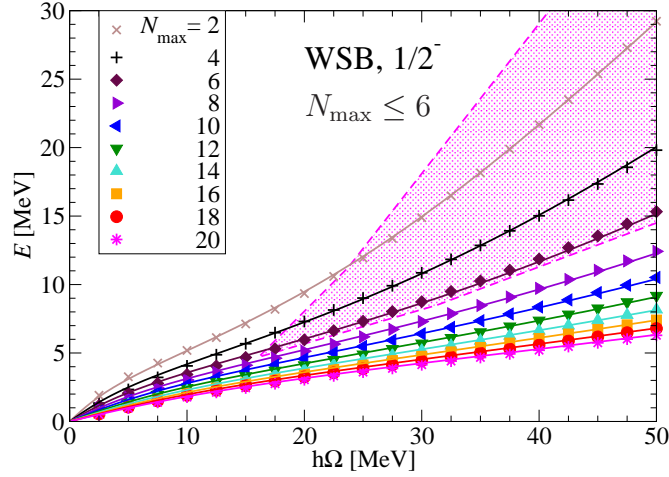


Figure 15: Selection of the lowest $\frac{1}{2}^-$ WSB eigenstates E_0 obtained with $N_{\max} \leq 6$. See Fig. 4 for details.

that contrary to the $\frac{3}{2}^-$ resonance we observe approximately 0.5 MeV differences between the resonance energy E_r and width Γ results obtained by the SS-HORSE technique and by numerical location of the respective S -matrix pole. We suppose that these differences originate from the fact that the $\frac{1}{2}^-$ resonance pole associated with this wide resonance is located far enough from the real energy axis; therefore the phase shifts even in the resonant region can be influenced by other S -matrix poles not accounted for by our phase shift parametrization (53).

We examine also a possibility of describing the $\frac{1}{2}^-$ phase shifts and resonance parameters by using only the eigenstates obtained with $N_{\max} \leq 6$ for our SS-HORSE analysis. We retain only these eigenstates from our previous selection as is shown by the shaded area in Fig. 15; this eigenstate selection is also illustrated by Fig. 16. The energies E_0 of all selected eigenstates are larger than the resonance region as is seen in Fig. 17. Nevertheless we reproduce the phase shifts and resonance parameters (see Fig. 17 and Table 2) nearly with the same accuracy as with the previous much more complete eigenstate selection. More, we accurately ‘predict’ eigenenergies in larger

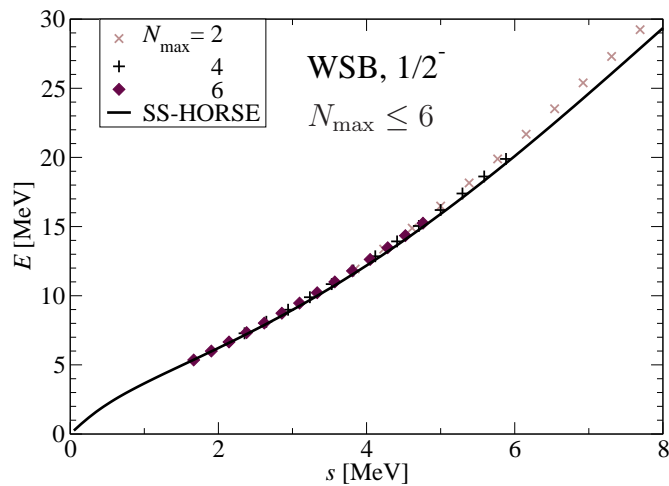


Figure 16: Selected lowest $\frac{1}{2}^-$ WSB eigenstates E_0 obtained with $N_{\max} \leq 6$ as a function of the scaling parameter s . See Fig. 5 for details.

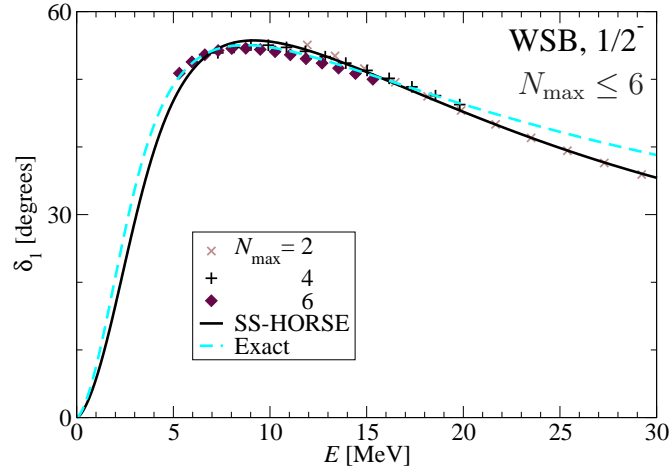


Figure 17: The $\frac{1}{2}^-$ WSB phase shifts generated by the selected eigenstates E_0 obtained with $N_{\max} \leq 6$. See Fig. 6 for details.

model spaces (see solid lines in Fig. 15) nearly with the same rms deviation as the fit involving those eigenstates as is indicated in Table 2.

3.3 Partial wave $\frac{1}{2}^+$

There are no resonances in the $n\alpha$ scattering in the $\frac{1}{2}^+$ partial wave. However, as it has been indicated in Ref. [14], the nuclear shell model should generate eigenstates in non-resonant energy intervals in continuum to be consistent with scattering observables. Therefore it is interesting to test with the WSB potential the ability of the SS-HORSE approach to describe the $\frac{1}{2}^+$ non-resonant $n\alpha$ scattering.

The low-energy $n\alpha$ scattering phase shifts in the $\frac{1}{2}^+$ state are described by Eq. (52). We shall see that to get the same quality fit as in the case of the odd-parity resonant scattering, we need in this case terms up to the 5th power of \sqrt{E} in the Taylor expansion of the background phase; therefore we preserve in Eq. (52) more terms than in Eq. (53). c , d and f are fitting parameters in Eq. (52). The WSB potential supports a bound state at energy E_b which mimics the Pauli-forbidden state in the $n\alpha$ scattering. We however treat E_b as an additional fitting parameter as a preparation to many-body NCSM calculations where it is impossible to obtain the energy of the Pauli-forbidden state. This bound state appears as the lowest state with negative energy obtained by the Hamiltonian diagonalization and is unneeded for our SS-HORSE analysis for which we use the first excited state $E_1 > 0$ which is the lowest state in the continuum.

The excitation quanta N_{\max} is conventionally used to define the many-body NCSM basis space while the total oscillator quanta \mathbb{N} is entering our SS-HORSE equations. The $\frac{1}{2}^+$ states in ${}^5\text{He}$ are unnatural parity states, hence N_{\max} takes odd values within NCSM, the minimal oscillator quanta $N_0 = 1$ in the five-body $n\alpha$ system, and

$$\mathbb{N} = N_{\max} + N_0 \quad (58)$$

is even. To retain a correspondence with NCSM, we are using N_{\max} to define the oscillator basis also in our model two-body problem. We note that in this case the N_{\max} is formally related to \mathbb{N} according to Eq. (27) where $\ell = 0$, and N_{\max} should be even for even \mathbb{N} . To have a closer correspondence with NCSM, we use Eq. (58) with $N_0 = 1$ within our model two-body problem instead of Eq. (27) to relate N_{\max} to \mathbb{N} , i.e., due to our NCSM-like definition, the $\frac{1}{2}^+$ eigenstates are labelled below by odd N_{\max}

values. Note, the definitions (27) and (58) result in the same N_{\max} in the case of odd-parity $\frac{3}{2}^-$ and $\frac{1}{2}^-$ $n\alpha$ partial waves.

Combining Eqs. (19), (52) and (58), we derive for the $n\alpha$ scattering in the $\frac{1}{2}^+$ partial wave:

$$-\frac{S_{N_{\max}+3,0}(E_\nu)}{C_{N_{\max}+3,0}(E_\nu)} = \tan\left(\pi - \arctan\sqrt{\frac{E_\nu}{|E_b|}} + c\sqrt{E_\nu} + d(\sqrt{E_\nu})^3 + f(\sqrt{E_\nu})^5\right), \quad (59)$$

where $\nu = 1$. We assign some values to the fitting parameters E_b , c , d and f and solve Eq. (59) to find a set of E_1 values, $\mathcal{E}_1^{(i)} = E_1(N_{\max}^i, \hbar\Omega^i)$, $i = 1, 2, \dots, D$, for each combination of N_{\max} and $\hbar\Omega$ and minimize the rms deviation from the selected eigenvalues $E_1^{(i)}$ obtained by the Hamiltonian diagonalization, see Eq. (57) where the subindex 0 should be replaced by 1, to find the optimal values of the fitting parameters.

The lowest continuum $\frac{1}{2}^+$ eigenstates E_1 of the model WSB Hamiltonian are shown as functions of $\hbar\Omega$ for various N_{\max} in Fig. 18 and as a function of the scaling parameter s in Fig. 19. All eigenenergies in this case seem to lie approximately on the same curve in Fig. 19; however, as in the case of odd parity partial waves, the deviations from the common curve are much more pronounced in the plot of the SS-HORSE phase shifts corresponding to these eigenstates (see Fig. 20) which clearly indicates the need to select eigenstates for the SS-HORSE fitting.

As in the case of the odd parity states, we use the $\Lambda > 385$ MeV/ c selection of eigenenergies as is illustrated by Fig. 21 and by the shaded area in Fig. 18. The obtained fitting parameters of Eq. (59) are presented in Table 3. It is interesting that the fitted energy E_b differs essentially from the exact value which is the energy of the bound state in the WSB potential. The SS-HORSE $\frac{1}{2}^+$ phase shifts nevertheless are seen in Fig. 22 to be nearly indistinguishable from the exact ones up to the energies of about 70 MeV where the SS-HORSE phase shifts governed by $N_{\max} = 1$ eigenstates slightly differ from exact. We note that the WSB bound state has a large binding energy, the respective S -matrix pole is far enough from the real momentum axis and hence has a minor influence on the phase shifts. This result indicates that one should not take seriously the energies of bound states obtained by the fit to the scattering data only, at least for well-bound states.

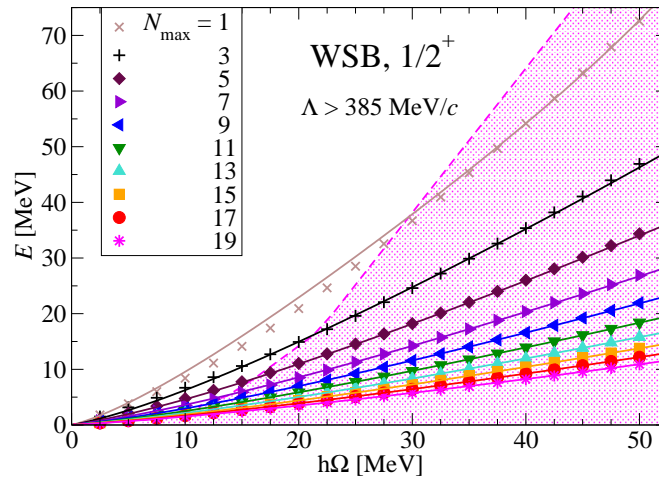


Figure 18: The lowest continuum $\frac{1}{2}^+$ WSB eigenstates E_1 as functions of $\hbar\Omega$ and their $\Lambda > 385$ MeV/ c selection. Solid lines are solutions of Eq. (59) for energies E_1 with parameters E_b , c , d and f obtained by the fit with this selection of eigenstates.

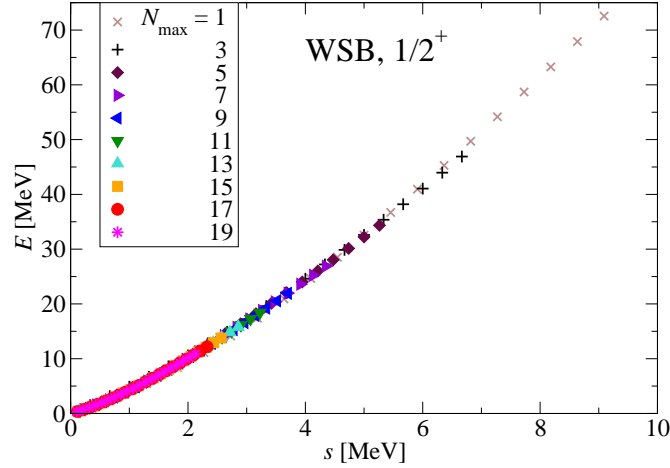


Figure 19: The lowest continuum $\frac{1}{2}^+$ WSB eigenstates E_1 as a function of the scaling parameter s .

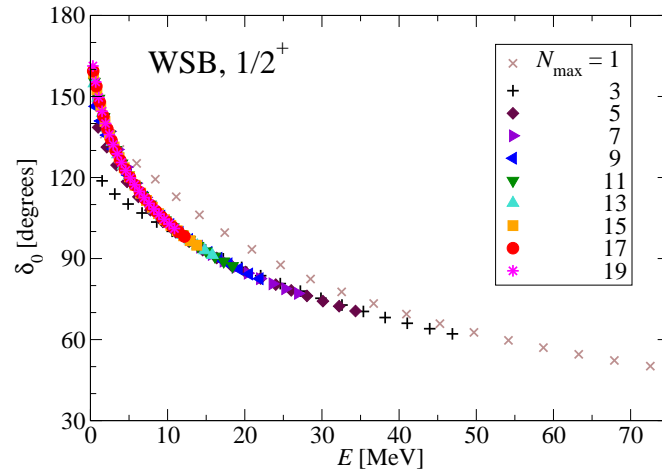


Figure 20: The $\frac{1}{2}^+$ phase shifts obtained directly from the WSB eigenstates E_1 using Eq. (19).

To examine a possibility of describing the low-energy $\frac{1}{2}^+$ phase shifts using only the diagonalization results in small basis spaces, we remove from the previous selection the eigenenergies E_1 obtained with $N_{\max} > 5$ as is illustrated by Figs. 23 and 24. We obtain nearly the same values of the fitting parameters as is seen from Table 3.

Table 3: $\frac{1}{2}^+$ $n\alpha$ scattering with model WSB potential: fitting parameters E_b , c , d and f of Eq. (59), rms deviation of fitted energies Ξ and the number of these fitted energies D for different selections of eigenvalues. For the $N_{\max} \leq 5$ selection, Ξ and D for all energies from the previous selection are shown within brackets.

Selection	E_b (MeV)	c (MeV $^{-\frac{1}{2}}$)	$d \cdot 10^3$ (MeV $^{-\frac{3}{2}}$)	$f \cdot 10^5$ (MeV $^{-\frac{5}{2}}$)	Ξ (keV)	D
$\Lambda > 385 \text{ MeV}/c$	-6.841	-0.157	+1.19	-0.888	163	151
$N_{\max} \leq 5$	-6.853	-0.156	+1.19	-0.888	332(163)	35(151)
Exact	-9.85					

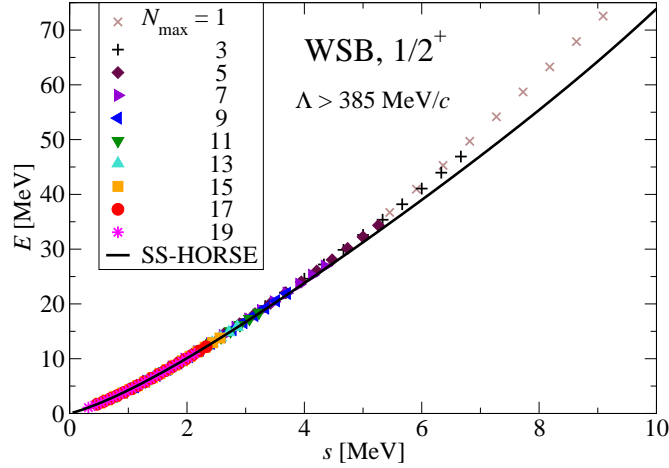


Figure 21: The $\Lambda > 385$ MeV/ c selected $\frac{1}{2}^+$ WSB eigenstates E_1 as a function of the scaling parameter s . The solid curve depicts solutions of Eq. (59) for energies E_1 with parameters E_b , c , d and f obtained by the fit with this selection of eigenstates.

The largest though still small enough difference is obtained for the fitted E_b values which, as has been already noted, does not play an essential role in the phase shifts. Therefore it is not surprising that we get an excellent description of the exact phase shifts presented in Fig. 25. Figure 23 demonstrates that we describe accurately not only the eigenstates E_1 involved in the fitting procedure but also those obtained in much larger basis spaces which were not fitted. The rms deviation in the description of energies of all $\Lambda > 385$ MeV/ c selected eigenstates is exactly the same as in the case when all these eigenstates were included in the fit.

As we already noted, the scaling of the eigenstates of finite Hamiltonian matrices in oscillator basis has been proposed by S. Coon and collaborators in Refs. [2, 3] who studied the convergence patterns of the bound states. They have demonstrated that the eigenenergies E_ν as functions of the scaling parameter $\lambda_{sc} \sim \sqrt{s}$ tend to a constant as λ_{sc} approaches 0; this constant is the convergence limit of the respective

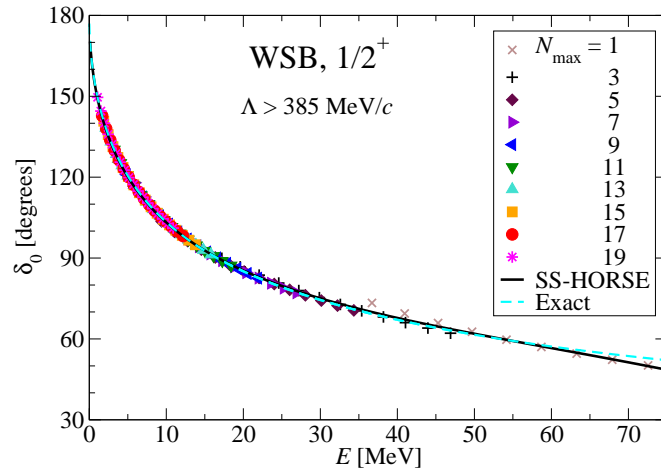


Figure 22: The $\frac{1}{2}^+$ WSB phase shifts generated by the $\Lambda > 385$ MeV/ c selected eigenstates E_1 (symbols). The solid curve depicts the phase shifts of Eq. (52) with parameters E_b , c , d and f obtained by the fit with this selection of eigenstates; the dashed curve is obtained by a numerical integration of the Schrödinger equation.

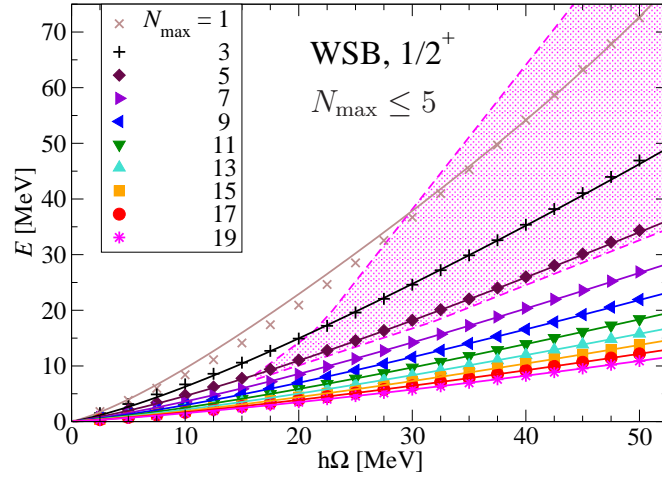


Figure 23: Selection of the lowest $\frac{1}{2}^+$ WSB eigenstates E_1 obtained with $N_{\max} \leq 5$. See Fig. 4 for details.

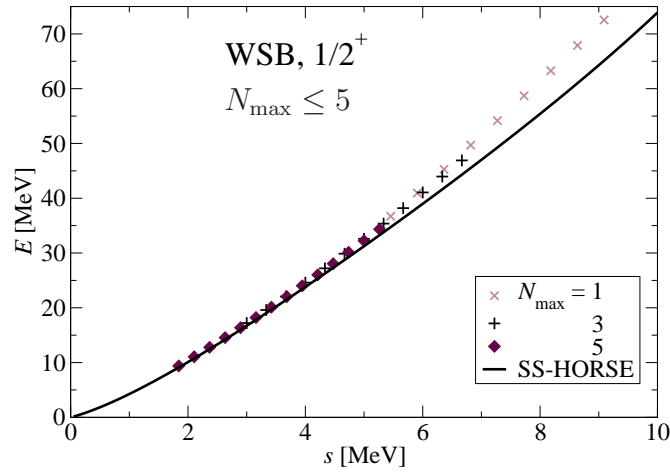


Figure 24: Selected lowest $\frac{1}{2}^+$ WSB eigenstates E_1 obtained with $N_{\max} \leq 5$ as a function of the scaling parameter s . See Fig. 21 for details.

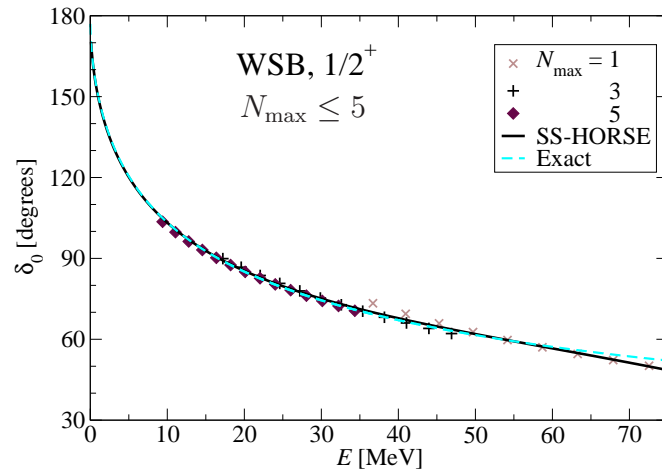


Figure 25: The $\frac{1}{2}^+$ WSB phase shifts generated by the selected eigenstates E_1 obtained with $N_{\max} \leq 6$. See Fig. 22 for details.

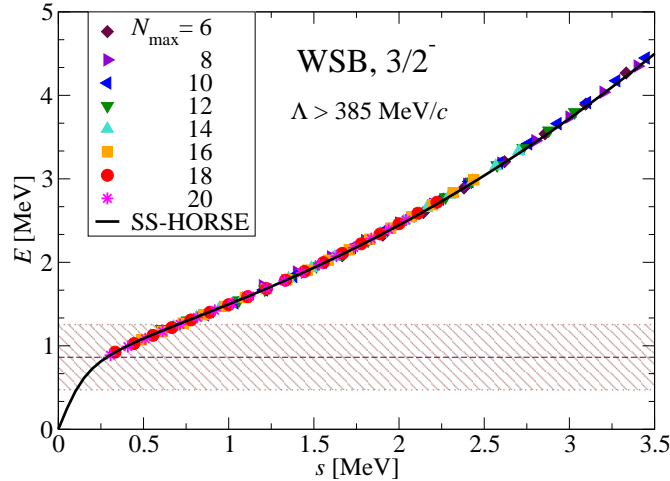


Figure 26: The same as Fig. 5 but in a larger scale. The dashed line corresponds to the resonance energy E_r , the shaded area shows the resonance width.

eigenenergy in the infinite basis. Our study extends the scaling patterns of the harmonic oscillator eigenstates to the case of states in the continuum. In this case the eigenenergies should approach 0 as the basis is expanded infinitely. The solid lines in Figs. 21 and 24 demonstrate the behaviour of eigenenergies in the continuum E_1 as a function of the scaling parameter s in the case of a system which has a bound state and does not have resonances in the low-energy region; the respective low-energy phase shifts are described by Eq. (52), a general formula for this case. The eigenstates are seen to be a smooth monotonic function of s (or λ_{sc}) which tends, as expected, to zero as $s \rightarrow 0$.

The solid lines in Figs. 5, 8, 13 and 16 demonstrate the behaviour of the eigenstates E_0 as a function of the scaling parameter s when the low-energy phase shifts are given by Eq. (53) which is a general formula describing a system which does not have a bound state but has a low-energy resonance. We see again a smooth monotonically increasing function of s with a large enough derivative at large s . At smaller s when the energy approaches the resonant region, the derivative of $E_0(s)$ decreases; this decrease of the derivative is more pronounced for narrow resonances as can be seen by comparing Figs. 5 and 13. Figure 26 where the function $E_0(s)$ from Fig. 5 is shown in a larger scale together with the resonant region, demonstrates that the further decrease of s strongly enhances the derivative of this function at the energies below the resonance energy E_r . When the function $E_0(s)$ leaves the resonant region at smaller s values, the next eigenstate $E_1(s)$ (not shown in the figure) approaches the resonant region from above.

These are the general convergence trends of the positive energy eigenstates obtained in the oscillator basis.

Concluding this section, we have demonstrated using the WSB potential as an example that the proposed SS-HORSE technique is adequate for the description of low-energy scattering phase shifts and resonance energies E_r and widths Γ . A very encouraging sign for many-body shell-model applications is that the resonance parameters and phase shifts can be obtained nearly without losing the accuracy by using within the SS-HORSE approach only the Hamiltonian eigenstates obtained in small basis spaces; more, having the low-lying energies from small basis spaces we are able to ‘predict’ accurately the values of eigenenergies in much larger oscillator bases.

4 SS-HORSE NCSM calculation of resonances in $n\alpha$ scattering

We discuss here the application of our SS-HORSE technique to $n\alpha$ scattering phase shifts and resonance parameters based on *ab initio* many-body calculations of ${}^5\text{He}$ within the NCSM with the realistic JISP16 NN interaction. The NCSM calculations are performed using the code MFDn [45, 46] with $2 \leq N_{\text{max}} \leq 18$ for both parities and with $\hbar\Omega$ values ranging from 10 to 40 MeV in steps of 2.5 MeV.

As it has been already noted above, for the SS-HORSE analysis we need the ${}^5\text{He}$ energies relative to the $n + \alpha$ threshold. Therefore from each of the ${}^5\text{He}$ NCSM odd (even) parity eigenenergies we subtract the ${}^4\text{He}$ ground state energy obtained by the NCSM with the same $\hbar\Omega$ and the same N_{max} (with $N_{\text{max}} - 1$) excitation quanta, and in what follows these subtracted energies are called NCSM eigenenergies E_ν . Only these ${}^5\text{He}$ NCSM eigenenergies relative to the $n + \alpha$ threshold are discussed below.

4.1 Partial wave $\frac{3}{2}^-$

We utilize the same Eq. (56) to fit the parameters describing the low-energy $\frac{3}{2}^-$ and $\frac{1}{2}^-$ phase shifts as in the model problem; the only difference is that the lowest energy eigenstates E_0 are obtained now from the many-body NCSM calculations. These lowest $\frac{3}{2}^-$ NCSM eigenstates are shown in Fig. 27 as functions of $\hbar\Omega$ for various N_{max} values. Figure 28 presents these eigenstates E_0 as a function of the scaling parameter s while Fig. 29 presents the $\frac{3}{2}^-$ phase shifts obtained directly from them using Eq. (19). Figures 28 and 29 clearly demonstrate the need of the eigenstate selection since many points in these figures deviate strongly from the common curves formed by other points. On the other hand, these figures demonstrate the convergence achieved in large N_{max} calculations: the deviation from the common curves occurs at smaller $\hbar\Omega$ values as N_{max} increases and all results from the largest available NCSM basis spaces seem to lie on the single common curves with the exception of only very few eigenenergies obtained with $\hbar\Omega < 15$ MeV.

Our first selection is the eigenstates fitting inequality $\Lambda > 600$ MeV/ c , the value

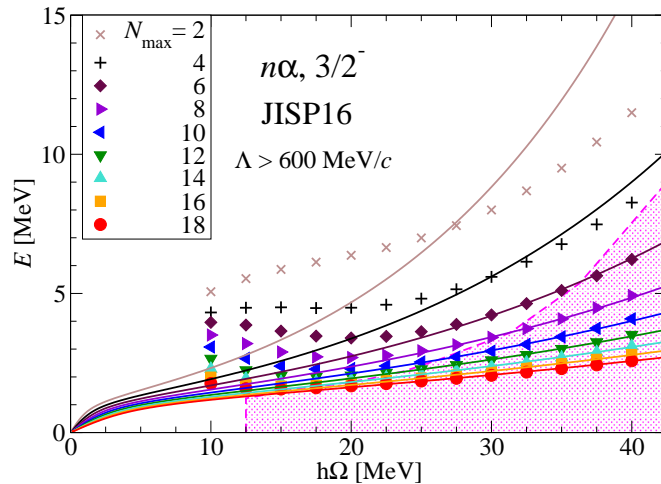


Figure 27: The lowest ${}^5\text{He}$ $\frac{3}{2}^-$ eigenstates E_0 obtained by the NCSM with various N_{max} as functions of $\hbar\Omega$. The shaded area shows the E_0 values selected for the SS-HORSE analysis according to inequality $\Lambda > 600$ MeV/ c . Solid lines are solutions of Eq. (56) for energies E_0 with parameters a , b and d obtained by the fit.

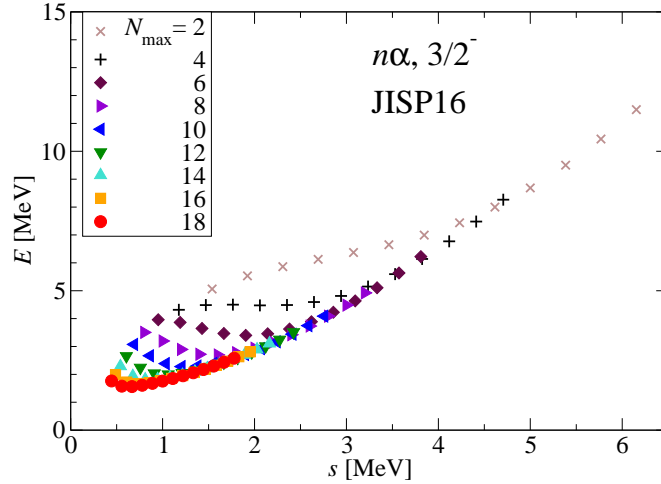


Figure 28: The lowest ${}^5\text{He } \frac{3}{2}^-$ eigenstates E_0 as a function of the scaling parameter s .

recommended in Refs. [2, 3] for the JISP16 NN interaction. This selection is illustrated by the shaded area in Fig. 27; common curves are formed by the selected eigenenergies E_0 plotted as a function of the scaling parameter s in Fig. 30 and by the phase shifts obtained directly from these eigenenergies with the help of Eq. (53) in Fig. 31. We get an accurate fit of the selected NCSM eigenenergies with the rms deviation of 31 keV, the obtained values of the fitting parameters a , b , d of Eq. (56) and the $\frac{3}{2}^-$ resonance energy E_r and width Γ are presented in Table 4. The fit accuracy is also illustrated by solid lines in Figs. 27, 30 and 31 obtained using our fitting parameters: these curves are seen to reproduce the selected NCSM energies E_0 in Figs. 27 and 30 and the corresponding phase shifts in Fig. 31.

The JISP16 NN interaction generates the $\frac{3}{2}^-$ phase shifts reproducing qualitatively but not quantitatively the results of phase shift analysis of Refs. [47] of $n\alpha$ scattering data as is seen in Fig. 31. We obtain the resonance energy E_r slightly above the experimental value, the difference is about 0.2 MeV (see Table 4). The resonance width Γ is also overestimated by JISP16, the difference between the JISP16 prediction and experiment is about 0.4 MeV. We present in Fig. 31 and in the last row of Table 4

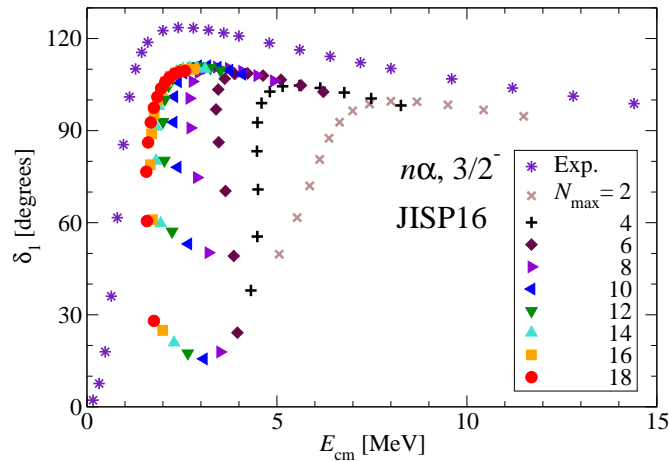


Figure 29: The $\frac{3}{2}^-$ $n\alpha$ phase shifts obtained directly from the ${}^5\text{He}$ eigenstates E_0 using Eq. (19) and the phase shift analysis of experimental data of Refs. [47] (stars).

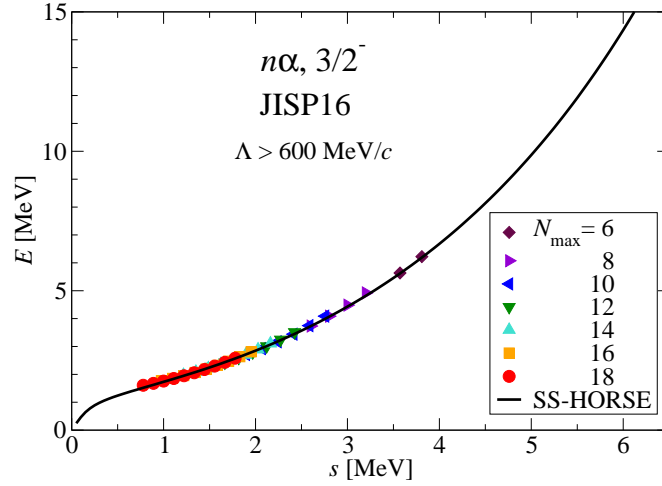


Figure 30: The ${}^5\text{He } \frac{3}{2}^-$ eigenstates E_0 selected according to $\Lambda > 600 \text{ MeV}/c$ plotted as a function of the scaling parameter s (symbols). See Fig. 5 for other details.

also the fit by Eq. (53) of the phase shift analysis of experimental data of Refs. [47] obtained by minimizing the rms deviation of the phase shifts (column Ξ in the Table). The fit parameters derived from the experimental data are seen to be markedly different from those derived from JISP16 by the NCSM-SS-HORSE approach.

Returning to the $\frac{3}{2}^-$ ${}^5\text{He}$ eigenstates depicted in Fig. 27, we see that the solid curves presenting our fit in this figure describe not only the selected eigenstates from the shaded area but also many other eigenstates not involved in the fit. This signals that the $\Lambda > 600 \text{ MeV}/c$ selection is too restrictive and we can use for the SS-HORSE analysis and fits many more NCSM eigenstates. We can use within the SS-HORSE approach all eigenstates forming with the others a common curve in Fig. 28 and especially in Fig. 29 which is, as we have noted, more sensitive to convergence patterns. There is however a restriction: unacceptable for the SS-HORSE are eigenstates E_ν

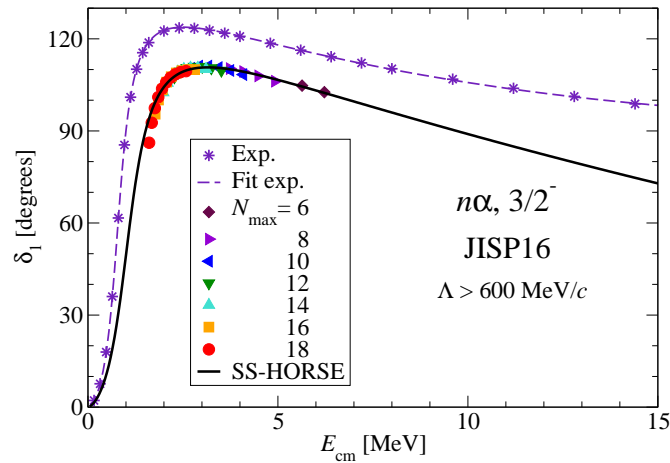


Figure 31: The $\frac{3}{2}^-$ $n\alpha$ phase shifts obtained using Eq. (19) directly from ${}^5\text{He}$ eigenstates E_0 selected according to $\Lambda > 600 \text{ MeV}/c$ (symbols). The solid curve depicts the phase shifts of Eq. (53) with parameters a , b and d obtained by the fit with the respective selection of eigenstates; stars and the dashed curve depict the phase shift analysis of experimental data of Refs. [47] and the fit by Eq. (53).

Table 4: $\frac{3}{2}^-$ resonance in $n\alpha$ scattering from the ${}^5\text{He}$ NCSM calculations with JISP16 NN interaction: fitting parameters a , b , d of Eq. (56), resonance energy E_r and width Γ , rms deviation of fitted energies Ξ and the number of these fitted energies D for different selections of eigenvalues in comparison with the analysis of experimental data in various approaches of Refs. [48] and [14] and with the fit by Eq. (53) of the phase shifts δ_1 extracted from experimental data in Ref. [47]. For the $N_{\max} \leq 4$ selection, Ξ and D for all energies from the manual selection are shown within brackets.

Selection	a (MeV $^{\frac{1}{2}}$)	b^2 (MeV)	$d \cdot 10^4$ (MeV $^{-\frac{3}{2}}$)	E_r (MeV)	Γ (MeV)	Ξ (keV)	D
$\Lambda > 600$ MeV/ c	0.505	1.135	-0.9	1.008	1.046	31	46
Manual	0.506	1.019	+93.2	0.891	0.989	70	68
$N_{\max} \leq 4$	0.515	1.025	+101	0.892	1.008	106(81)	11(68)
Nature:							
R -matrix [48]				0.80	0.65		
J -matrix [14]				0.772	0.644		
Fit δ_1 of Ref. [47]	0.358	0.839	+55.9	0.774	0.643	0.21 $^\circ$	26

obtained with any given N_{\max} from the range of $\hbar\Omega$ values where their energy decreases with $\hbar\Omega$, i. e., we can select only those eigenstates with a given fixed N_{\max} which derivative $\frac{E_\nu}{\hbar\Omega} > 0$ — Eqs. (56) and (59) do not exclude mathematically the possibility of having $\frac{E_\nu}{\hbar\Omega} < 0$ but such solutions can arise only with unphysical parameters of these equations.

We would like to use within the SS-HORSE as many NCSM eigenstates as possible in order to enlarge the energy interval where the phase shifts are fitted and to improve the accuracy of the fit parameters. From this point of view, the selection according to inequality $\Lambda > \Lambda_0$ is not favorable. The $\Lambda > \Lambda_0$ rule excludes states with $\hbar\Omega < \hbar\Omega_0$ where $\hbar\Omega_0$ depends on N_{\max} and decreases as N_{\max} increases. As is seen from our study of the model problem, in particular, from Figs. 3, 4, 10, 12, 18, 20, we can utilize for the SS-HORSE the eigenstates obtained with sufficiently large N_{\max} and with very small $\hbar\Omega$; the same conclusion follows from our *ab initio* many-body study of the system of four neutrons (tetra-neutron) in the continuum [49,50]. According to the $\Lambda > \Lambda_0$ rule we either exclude these large N_{\max} – small $\hbar\Omega$ eigenstates or include in the fit some small N_{\max} states which strongly deviate from common curves on the plots of E_ν vs s or δ_ℓ vs E .

The ultraviolet cutoff Λ_0 was introduced in Refs. [2,3] with an idea that the oscillator basis should be able to describe in the many-body system the short-range (high-momentum) behaviour of the two-nucleon interaction employed in the calculations; thus the $\hbar\Omega$ cannot be too small since oscillator functions with small $\hbar\Omega$ have a large radius (correspond to small momentum) and are not able to catch the short-range (high-momentum) peculiarities of a particular NN potential. We imagine this concept to be insufficient at least in some cases. In light nuclei where binding energies are not large, the structure of the wave function can be insensitive to the short-range NN potential behaviour associated with high relative momentum. Much more important is the radius of the state under consideration, e. g., we can expect an adequate description of the ground state only if the highest oscillator function in the basis has at least one node within the radius of this state, two nodes are required within the radius of the first excited state, etc. Therefore the minimal acceptable $\hbar\Omega$ value depends strongly on the state under consideration and may be insensitive to the inter-nucleon interaction. This is particularly important for loosely-bound nuclear states or for low-energy scattering states. In the case of scattering, the wave function at low energies can have a very distant first node and not only permits but just

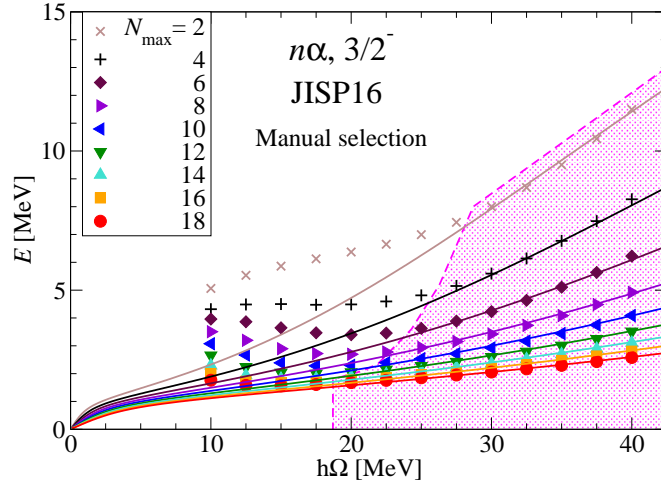


Figure 32: Manual selection the lowest ${}^5\text{He } \frac{3}{2}^-$ eigenstates E_0 . See Fig. 27 for details.

requires the use of oscillator functions with very small $\hbar\Omega$ values and large radius.

We cannot formulate a simple rule or formula for selecting eigenstates acceptable for the SS-HORSE analysis, instead we pick up manually individual states with eigenenergies E_0 lying to the right from the minimum of the $\hbar\Omega$ dependence for each N_{max} in Fig. 27 and lying on or close to the common curve in Figs. 28 and 29. These manually selected eigenstates and the respective phase shifts are presented in Figs. 32, 33 and 34. The results of the fit with this selection of eigenstates are presented in the second line of Table 4. We obtain an accurate fit with the rms deviation of eigenenergies of 70 keV; this number however depends on the selection criteria like the acceptable distance from the common curve formed by other points in Figs. 33 and 34. Comparing Figs. 27 and 32 we see that our manual selection makes it possible to describe eigenenergies with small N_{max} which were far from theoretical curves in Fig. 27. These small N_{max} states have large energies, and their inclusion in the SS-HORSE analysis extends the description of the phase shifts in the high-energy region in Fig. 34 pushing them closer to the phase shift analysis of the experimental

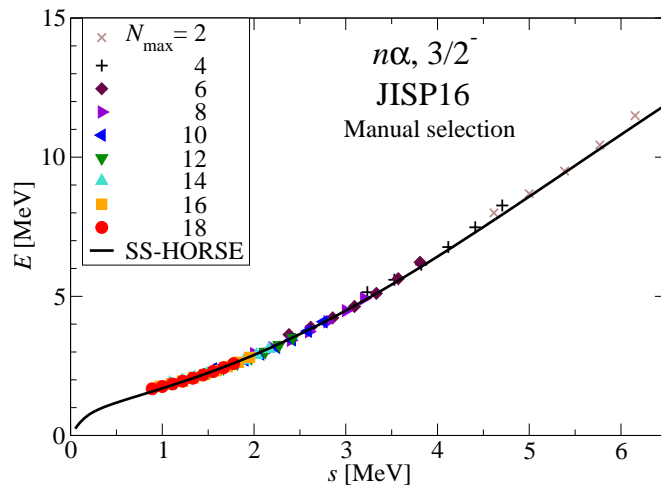


Figure 33: Manually selected ${}^5\text{He } \frac{3}{2}^-$ eigenstates E_0 plotted as a function of the scaling parameter s (symbols). See Fig. 5 for other details.

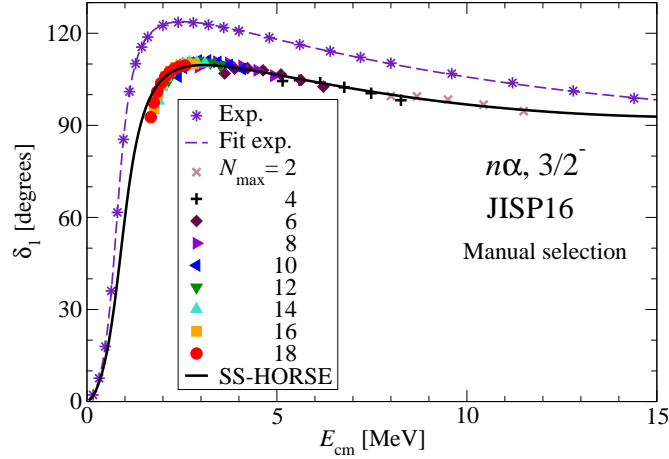


Figure 34: The $\frac{3}{2}^-$ $n\alpha$ phase shifts generated by the manually selected ${}^5\text{He}$ eigenstates E_0 . See Fig. 31 for details.

$n\alpha$ scattering data in this region as compared with Fig. 31. These changes in the phase shift behavior at larger energies correspond to a drastic change of the fitting parameter d which is the coefficient of the highest power term in the expansion (53). At smaller energies including the resonance region, the phase shifts obtained from the fits with the manual and with the $\Lambda > 600$ MeV/ c selections are nearly the same, and we get close values of the respective fitting parameters a and b and hence small changes of the resonance energy E_r and width Γ due to the switch from one selection to the other.

It is very interesting to investigate whether we can get reasonable phase shifts and resonance parameters using only the NCSM eigenstates from small basis spaces. From our manually selected eigenstates we select only those obtained with $N_{\text{max}} = 2$ and 4. This selection and the results obtained by the fit are depicted in Figs. 35, 36 and 37. All eigenenergies E_0 involved in this fit are significantly above the resonant region (see Fig. 37). Nevertheless we obtain from these 11 small- N_{max} eigenstates nearly the same phase shifts as those from all 68 manually selected eigenstates and

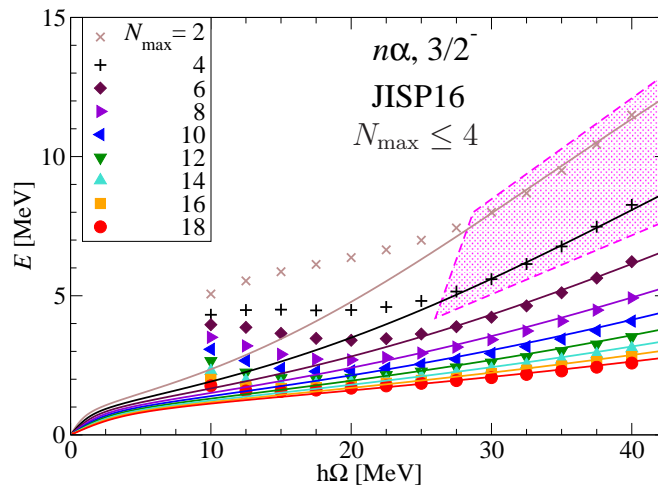


Figure 35: Selection of the lowest ${}^5\text{He}$ $\frac{3}{2}^-$ eigenstates E_0 obtained in NCSM with $N_{\text{max}} \leq 4$. See Fig. 27 for details.

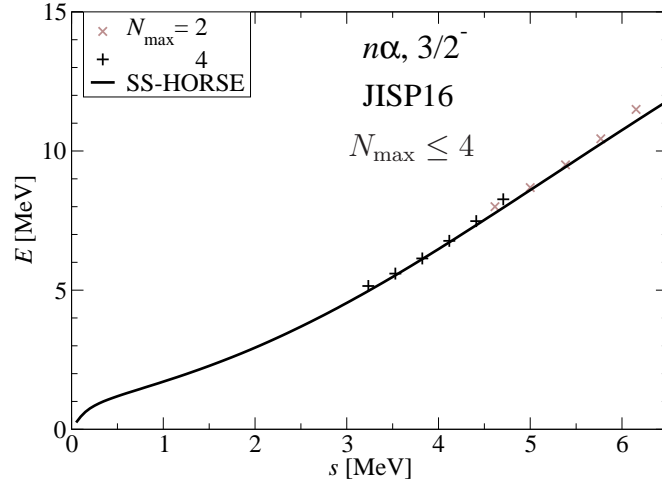


Figure 36: Selected lowest ${}^5\text{He } \frac{3}{2}^-$ eigenstates E_0 obtained in NCSM with $N_{\text{max}} \leq 4$ as a function of the scaling parameter s . See Fig. 5 for other details.

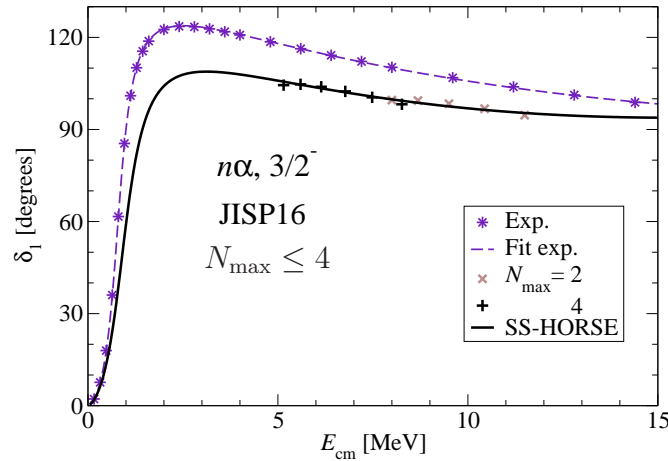


Figure 37: The $\frac{3}{2}^-$ $n\alpha$ phase shifts generated by the selected ${}^5\text{He}$ eigenstates E_0 obtained in NCSM with $N_{\text{max}} \leq 4$. See Fig. 31 for details.

very close values of fit parameters and of the resonance energy and width presented in Table 4. Figure 35 demonstrates that, as in the case of the model problem, with these eigenstates E_0 from many-body NCSM calculations with $N_{\text{max}} \leq 4$ we can accurately ‘predict’ the ${}^5\text{He}$ eigenstates obtained in much larger basis spaces and in a wider range of $\hbar\Omega$. The rms deviation Ξ of all manually selected eigenstates by this $N_{\text{max}} \leq 4$ fit is only 81 keV as compared with 70 keV from the fit to all those eigenstates.

4.2 Partial wave $\frac{1}{2}^-$

The lowest $\frac{1}{2}^-$ eigenstates of ${}^5\text{He}$ from the NCSM calculations with JISP16 NN interaction are presented in Fig. 38 as functions of $\hbar\Omega$ and in Fig. 39 as a function of the scaling parameter s , Fig. 40 presents the respective $n\alpha$ phase shifts. The eigenenergies in Figs. 39 and 40 tend to form single common curves demonstrating the convergence in many-body NCSM calculations, however we see that many eigenstates diverge from the common curves and lie far from them thus demonstrating the need to select the states for the SS-HORSE analysis.

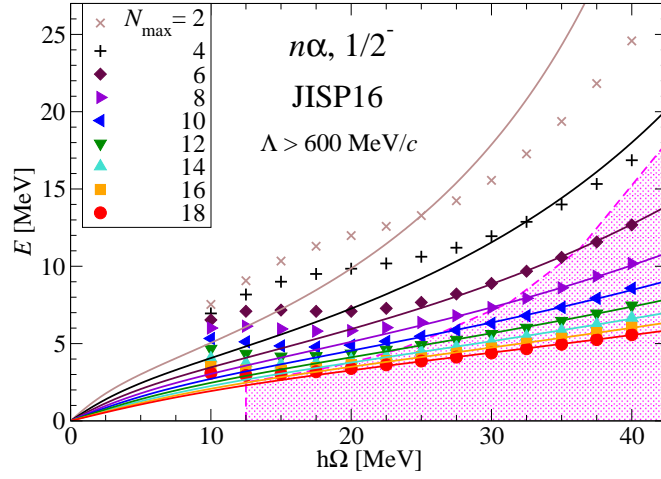


Figure 38: The lowest ${}^5\text{He } \frac{1}{2}^-$ eigenstates E_0 as functions of $\hbar\Omega$ and their $\Lambda > 600$ MeV/c selection. See Fig. 27 for details.

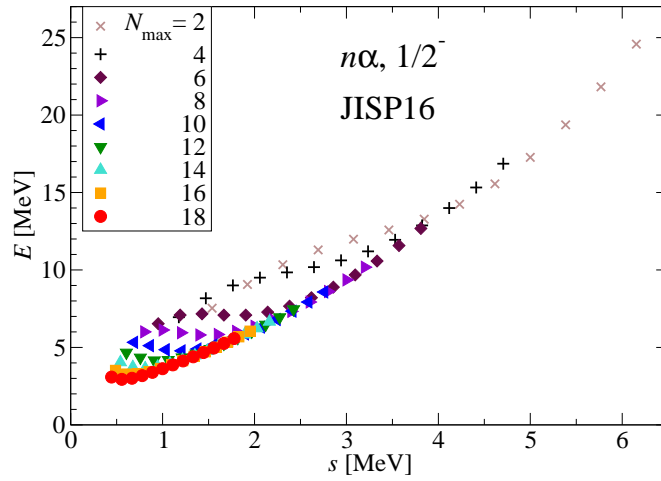


Figure 39: The lowest ${}^5\text{He } \frac{1}{2}^-$ eigenstates E_0 as a function of the scaling parameter s .

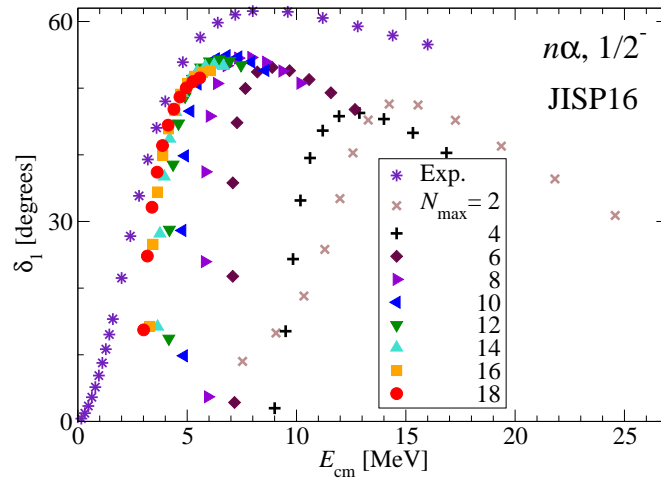


Figure 40: The $\frac{1}{2}^-$ $n\alpha$ phase shifts obtained directly from the ${}^5\text{He}$ eigenstates E_0 using Eq. (19). See Fig. 29 for other details.

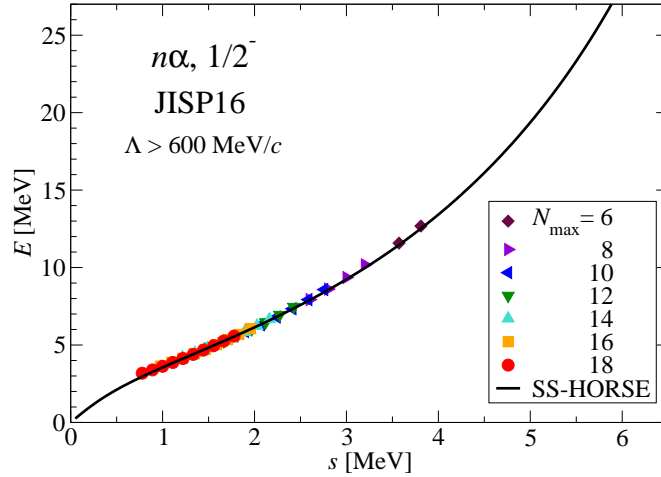


Figure 41: The ${}^5\text{He } \frac{1}{2}^-$ eigenstates E_0 selected according to $\Lambda > 600 \text{ MeV}/c$ as a function of the scaling parameter s . See Fig. 5 for other details.

As in the case of the $\frac{3}{2}^-$ partial wave, we start from the $\Lambda > 600 \text{ MeV}/c$ eigenstate selection recommended for the JISP16 NN interaction in Refs. [2, 3] which is illustrated in Figs. 38 and 41, the respective phase shifts are shown in Fig. 42. The selected states form reasonably smooth common curves in Figs. 41 and 42 making possible an accurate fit of parameters in Eq. (53); the obtained fitted parameters can be found in Table 5. We get a good description of the $\frac{1}{2}^-$ resonance energy and width however the phase shift behaviour extracted from the experimental $n\alpha$ scattering data is reproduced qualitatively but not quantitatively (see Fig. 42). Note however that the fit parameters derived from the experimental data and JISP16 results (Table 5) are close with the exception of the parameter d which contribution is very small at energies below 20 MeV. Figure 38 shows that we reproduce not only the eigenstate energies from the shaded area that were fitted but also many other eigenstates not included in the fit, especially small- N_{max} eigenstates, thus suggesting to perform a manual eigenstate selection which will involve many more eigenenergies in the SS-HORSE analysis.

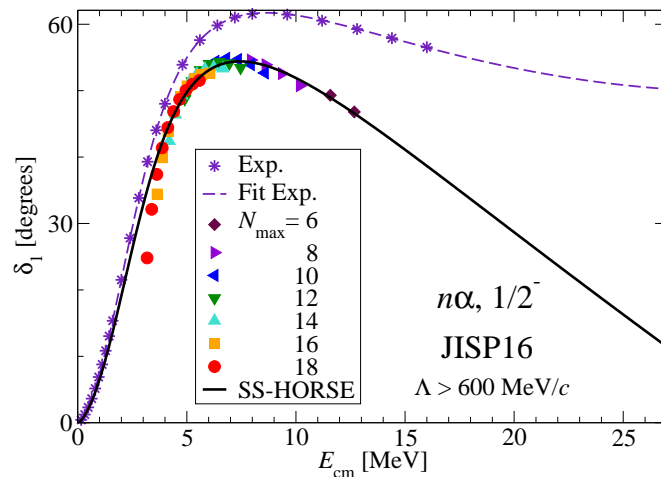


Figure 42: The $\frac{1}{2}^-$ $n\alpha$ phase shifts generated by the $\Lambda > 600 \text{ MeV}/c$ selected ${}^5\text{He}$ eigenstates E_0 . See Fig. 31 for details.

Table 5: Parameters of the $\frac{1}{2}^-$ resonance in $n\alpha$ scattering from the ${}^5\text{He}$ NCSM calculations with JISP16 NN interaction. See Table 4 for details.

Selection	a ($\text{MeV}^{\frac{1}{2}}$)	b^2 (MeV)	$d \cdot 10^4$ ($\text{MeV}^{-\frac{3}{2}}$)	E_r (MeV)	Γ (MeV)	Ξ (keV)	D
$\Lambda > 600 \text{ MeV}/c$	1.680	3.443	-3.6	2.031	5.559	61	46
Manual	1.699	3.299	21.3	1.856	5.456	11	60
$N_{\max} \leq 4$	2.460	6.734	-0.15	3.710	11.24	109(893)	9(60)
$4 \leq N_{\max} \leq 6$	1.718	3.310	25.0	1.834	5.511	25(92)	10(60)
Nature:							
R -matrix [48]				2.07	5.57		
J -matrix [14]				1.97	5.20		
Fit δ_1 of Ref. [47]	1.622	3.276	+46.3	1.960	5.249	0.038°	26

Our manual selection of the lowest $\frac{1}{2}^-$ eigenstates in ${}^5\text{He}$ is shown in Figs. 43 and 44 while the respective $n\alpha$ phase shifts are presented in Fig. 45, the results of the fit are given in Table 5. As in the case of the $\frac{3}{2}^-$ $n\alpha$ partial wave, the inclusion of the additional eigenstates in the fit does not affect the phase shifts at smaller energies including the resonance region. However, including the additional eigenstates pushes the phase shifts up in the direction of the phase shift analysis at larger energies. The $\frac{1}{2}^-$ resonance energy and width and the parameters of the phase shift fit by Eq. (53) are seen from Table 5 to change only slightly with the exception of the parameter d responsible for the phase shift behaviour at higher energies.

It is very interesting and important to examine whether it is possible to get a reasonable description of the resonance and phase shifts in the $\frac{1}{2}^-$ $n\alpha$ scattering using only eigenstates obtained in many-body NCSM calculations in small bases. In the case of the $\frac{3}{2}^-$ $n\alpha$ scattering we manage to derive very good phase shifts from the $N_{\max} \leq 4$ NCSM eigenstates. Therefore we try the $N_{\max} \leq 4$ eigenstate selection also in the $\frac{1}{2}^-$ partial wave, see Figs. 46, 47 and 48. This selection clearly fails to reproduce the phase shifts and resonance parameters which differ essentially from the converged results obtained with the manual selection of the $\frac{1}{2}^-$ ${}^5\text{He}$ eigenstates (see Fig. 31 and Table 5); we see also in Fig. 46 that the fit to the $N_{\max} \leq 4$ eigenstates

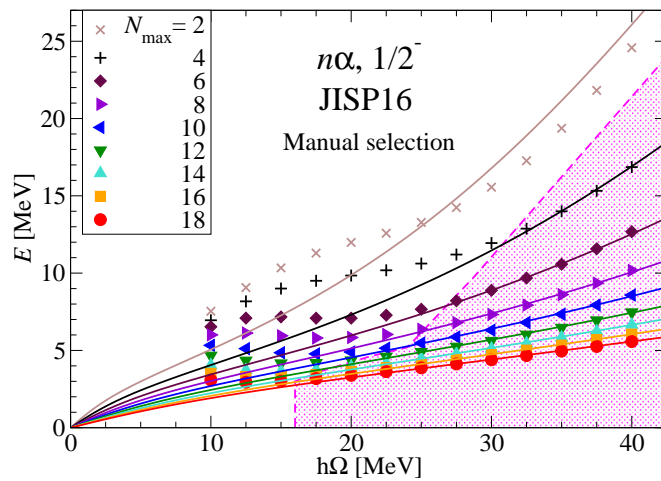


Figure 43: Manual selection the lowest ${}^5\text{He}$ $\frac{1}{2}^-$ eigenstates E_0 . See Fig. 27 for details.

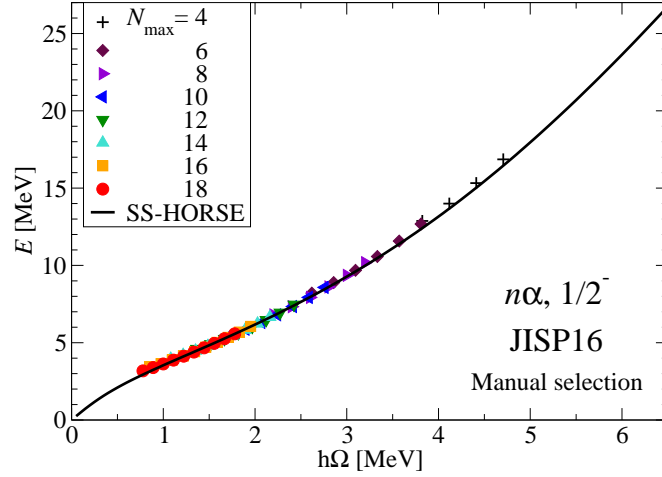


Figure 44: Manually selected ${}^5\text{He } \frac{1}{2}^-$ eigenstates E_0 plotted as a function of the scaling parameter s (symbols). See Fig. 5 for other details.

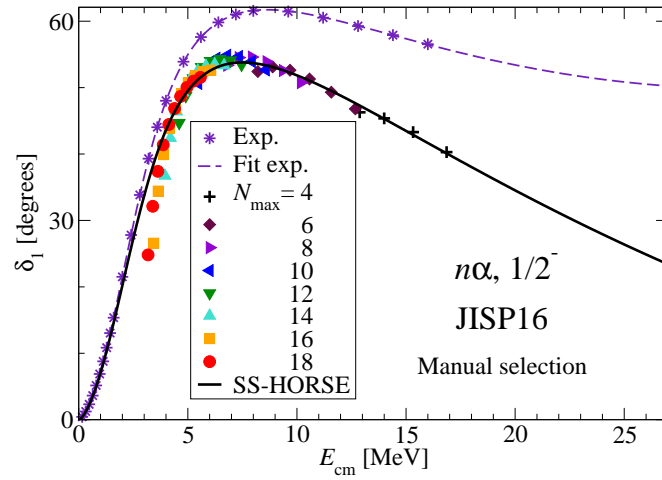


Figure 45: The $\frac{1}{2}^-$ $n\alpha$ phase shifts generated by the manually selected ${}^5\text{He}$ eigenstates E_0 . See Fig. 31 for details.

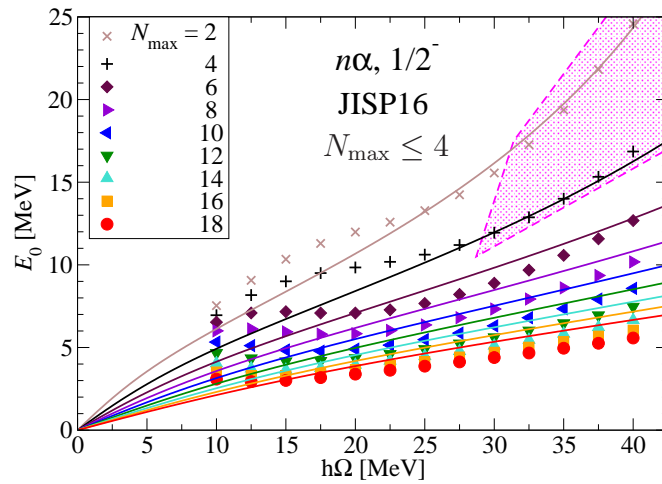


Figure 46: Selection of the lowest ${}^5\text{He } \frac{1}{2}^-$ eigenstates E_0 obtained in NCSM with $N_{\max} \leq 4$. See Fig. 27 for details.

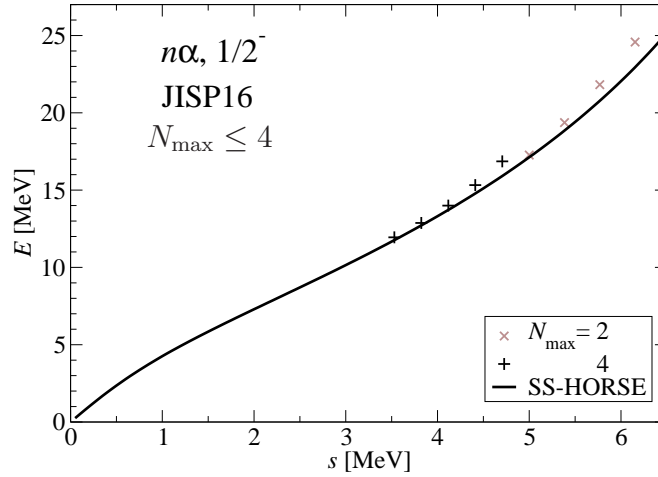


Figure 47: Selected lowest ${}^5\text{He } \frac{1}{2}^-$ eigenstates E_0 obtained in NCSM with $N_{\max} \leq 4$ as a function of the scaling parameter s . See Fig. 5 for other details.

from the shaded area fails to ‘predict’ the eigenenergies E_0 obtained with larger N_{\max} values. That is not surprising because the plots of the $N_{\max} \leq 4$ eigenenergies as a function of the scaling parameter s (Fig. 47) and of the respective phase shifts as a function of energy (Fig. 48) do not form smooth common curves.

However an entirely different result is obtained by selecting for the SS-HORSE analysis the ${}^5\text{He } \frac{1}{2}^-$ NCSM results from basis spaces with $4 \leq N_{\max} \leq 6$. For the $4 \leq N_{\max} \leq 6$ selection we pick up 10 eigenstates with the smallest N_{\max} values out of 60 manually selected before $\frac{1}{2}^-$ eigenstates. This eigenstate selection and the respective results are illustrated by Figs. 49, 50 and 51. The selected eigenenergies are seen to form sufficiently smooth curves in Figs. 50 and 51. The parameter fit results in nearly the same phase shifts (Fig. 51) as in the case of the manual eigenstate selection, we get also very close values of the resonance energy and width and fitting parameters listed in Table 5. Figure 49 demonstrates that by using only 10

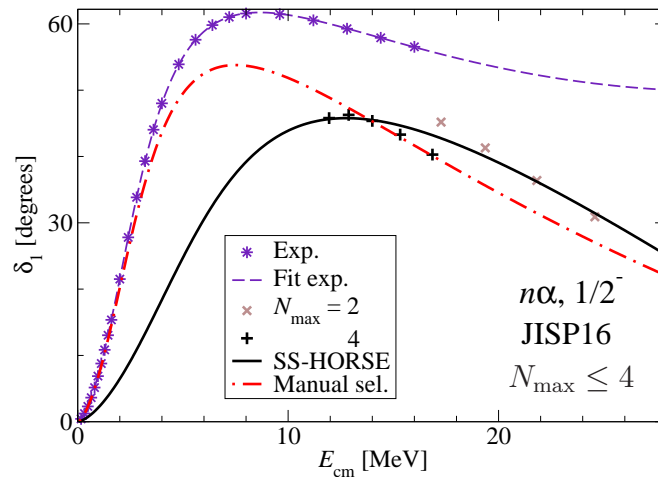


Figure 48: The $\frac{1}{2}^-$ $n\alpha$ phase shifts generated by the selected ${}^5\text{He}$ eigenstates E_0 obtained in NCSM with $N_{\max} \leq 4$. The dash-dotted curve depicts the phase shifts obtained by the fit to all manually selected eigenstates. See Fig. 31 for other details.

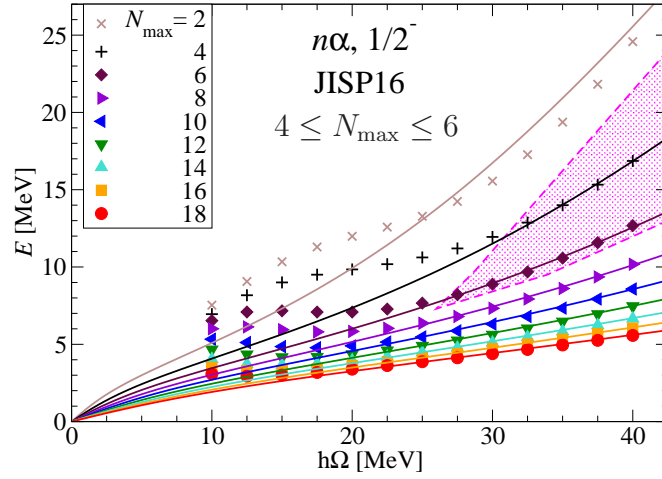


Figure 49: Selection of the lowest ${}^5\text{He } \frac{1}{2}^-$ eigenstates E_0 obtained in NCSM with $4 \leq N_{\max} \leq 6$. See Fig. 27 for details.

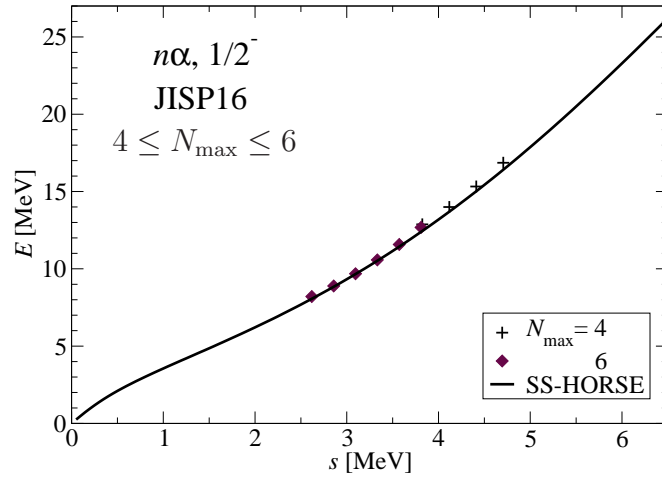


Figure 50: Selected lowest ${}^5\text{He } \frac{1}{2}^-$ eigenstates E_0 obtained in NCSM with $4 \leq N_{\max} \leq 6$ as a function of the scaling parameter s . See Fig. 5 for other details.

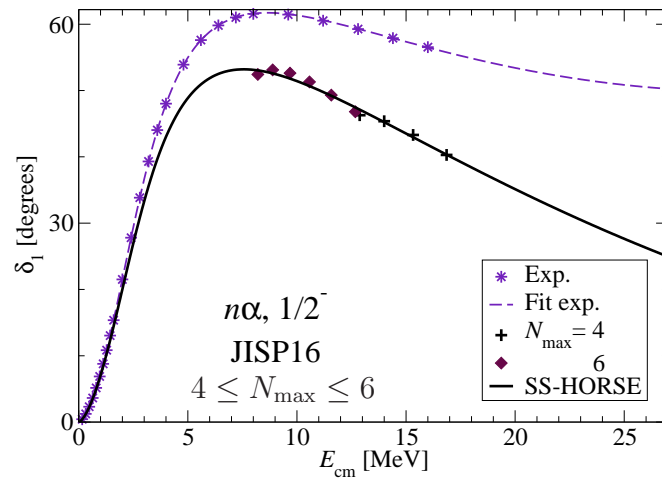


Figure 51: The $\frac{1}{2}^- n\alpha$ phase shifts generated by the selected ${}^5\text{He}$ eigenstates E_0 obtained in NCSM with $4 \leq N_{\max} \leq 6$. See Fig. 31 for details.

small- N_{\max} eigenstates from the shaded area we accurately ‘predict’ the energies of many higher- N_{\max} eigenstates: the rms deviation Ξ of energies of all 60 manually selected eigenstates is 92 keV (see Table 5). Of course, 92 keV is much larger than the Ξ value of 11 keV obtained in the full fit to all these 60 eigenenergies, but it is still an indication of a good quality ‘prediction’ of many-body eigenenergies E_0 obtained with much larger bases in a wide range of $\hbar\Omega$ values.

4.3 Partial wave $\frac{1}{2}^+$

In this subsection we examine a possibility to describe neutron-nucleus non-resonant scattering using as input for the SS-HORSE analysis the results of many-body shell model calculations. The SS-HORSE fit is done in the same manner as in the case of resonant scattering. The difference is that the non-resonant low-energy $n\alpha$ scattering phase shifts in the $\frac{1}{2}^+$ state are described by Eq. (52) instead of Eq. (53) which parameters are fitted using Eq. (59) instead of Eq. (56). The parameter E_b of this equation mimics the Pauli-forbidden state in the $n\alpha$ scattering. As compared with the discussion of the $\frac{1}{2}^+$ scattering by the model WSB potential which supports the Pauli-forbidden state, this bound state does not appear as a result of the NCSM ${}^5\text{He}$ calculations. Therefore we should use for the SS-HORSE fit the lowest $\frac{1}{2}^+$ state obtained by the NCSM with the eigenenergy E_0 and set $\nu = 0$ in Eq. (59).

These lowest $\frac{1}{2}^+$ ${}^5\text{He}$ eigenstates E_0 are shown as functions of $\hbar\Omega$ for various N_{\max} in Fig. 52 and as a function of the scaling parameter s in Fig. 53. We see a tendency of eigenstates to approach the common curve at smaller $\hbar\Omega$ values with increasing N_{\max} which signals that the convergence is achieved at smaller energies in larger basis spaces. This tendency is much more pronounced in the plot of the SS-HORSE phase shifts corresponding to the NCSM eigenstates in Fig. 54. This figure however also clearly indicates the need to select eigenstates for the SS-HORSE fitting.

We start with selecting eigenstates according to the inequality $\Lambda > 600 \text{ MeV}/c$ as is illustrated by Figs. 52 and 55, the respective phase shifts are shown in Fig. 56, and the obtained fitting parameters are presented in Table 6. We obtain a reasonable accuracy of the fit with the rms deviation of the fitted energies of 85 keV. We reproduce reasonably the phase shift behaviour by the JISP16 NN interaction. We note that at energies $E_{\text{cm}} > 25 \text{ MeV}$ the fit by Eq. (52) of the results of the phase shift analysis start going up with the energy. This seems unphysical, however the $\frac{1}{2}^+$

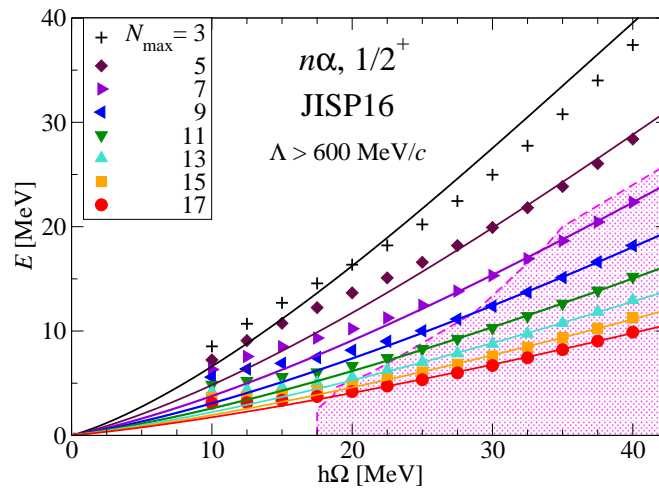


Figure 52: The lowest ${}^5\text{He}$ $\frac{1}{2}^+$ eigenstates E_0 as functions of $\hbar\Omega$ and their $\Lambda > 600 \text{ MeV}/c$ selection. See Fig. 18 for details.

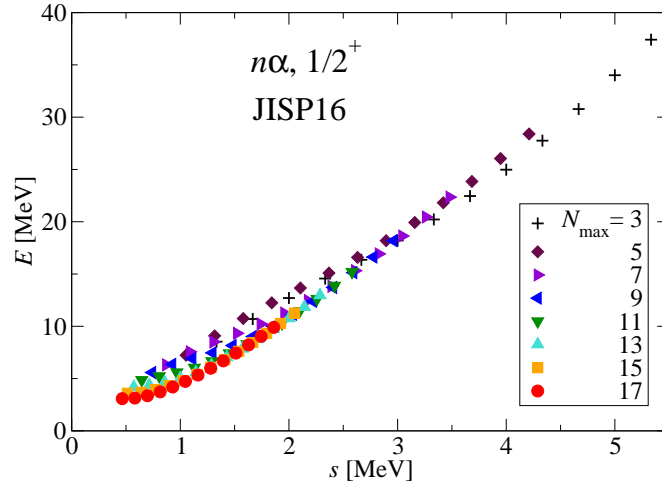


Figure 53: The lowest ${}^5\text{He } \frac{1}{2}^+$ eigenstates E_0 as a function of the scaling parameter s .

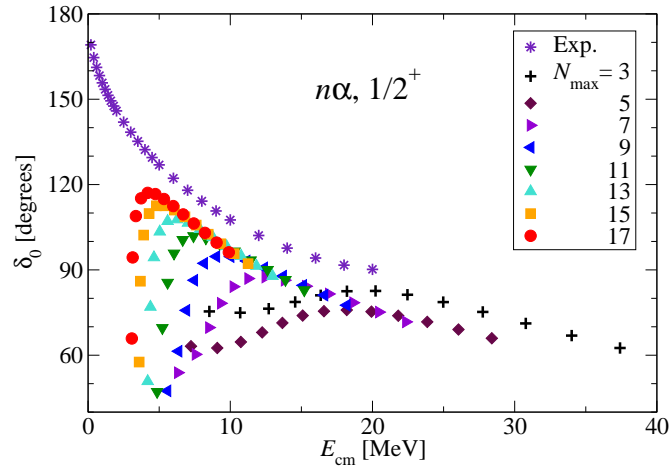


Figure 54: The $\frac{1}{2}^+$ $n\alpha$ phase shifts obtained directly from the ${}^5\text{He}$ eigenstates E_0 using Eq. (19). See Fig. 29 for other details.

Table 6: $\frac{1}{2}^+$ $n\alpha$ scattering from the ${}^5\text{He}$ NCSM calculations with JISP16 NN interaction: fitting parameters E_b , c , d and f of Eq. (59), rms deviation of fitted energies Ξ and the number of these fitted energies D for different selections of eigenvalues in comparison with the fit by Eq. (52) of the phase shifts δ_0 extracted from experimental data in Ref. [47]. For the $5 \leq N_{\max} \leq 7$ selection, Ξ and D for all energies from the manual selection are shown within brackets.

Selection	E_b (MeV)	c (MeV $^{-\frac{1}{2}}$)	$d \cdot 10^3$ (MeV $^{-\frac{3}{2}}$)	$f \cdot 10^5$ (MeV $^{-\frac{5}{2}}$)	Ξ (keV)	D
$\Lambda > 600 \text{ MeV}/c$	-5.996	-0.171	-8.02	6.48	85	41
Manual	-6.733	-0.183	-13.0	30.8	120	53
$5 \leq N_{\max} \leq 7$	-3.347	-0.151	63.0	-86.7	168(259)	13(53)
Fit δ_0 of Ref. [47]	-13.75	-0.156	-429	220	0.018°	26

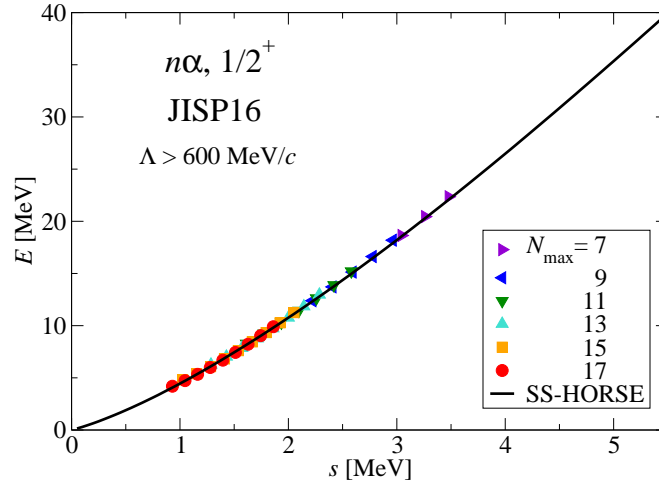


Figure 55: The ${}^5\text{He } \frac{1}{2}^+$ eigenstates E_0 selected according to $\Lambda > 600 \text{ MeV}/c$ as a function of the scaling parameter s . See Fig. 21 for other details.

phases extracted from the $n\alpha$ scattering data are available only up to $E_{\text{cm}} = 20 \text{ MeV}$; the phase shift analysis at higher energies is needed to obtain a more realistic fit in this energy interval where the NCSM-SS-HORSE phase shifts look more realistic.

Figure 52 demonstrates that it would be reasonable to perform a manual selection and to include in the fit more eigenstates thus extending the energy interval of the fitted phase shifts. Our manual selection of the lowest $\frac{1}{2}^+$ ${}^5\text{He}$ eigenstates and the respective phase shifts are presented in Figs. 57, 58, 59 and Table 6. Some of the fitting parameters are profoundly altered due to the inclusion of additional eigenstates in the fit, however the resulting phase shifts are nearly the same with an exception of the energies $E_{\text{cm}} > 30 \text{ MeV}$ where these additional eigenstates push the phase shifts slightly up. The phase shift analysis is unavailable at these energies, therefore it is impossible to judge whether this adjustment of the phase shifts improves the description of the experiment.

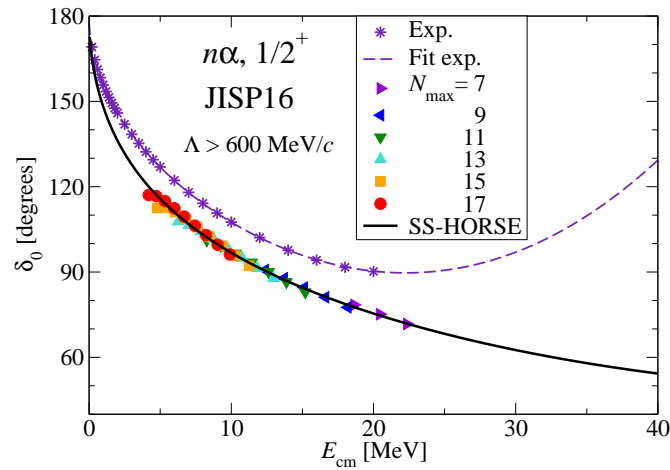


Figure 56: The $\frac{1}{2}^+$ $n\alpha$ phase shifts generated by the $\Lambda > 600 \text{ MeV}/c$ selected ${}^5\text{He}$ eigenstates E_0 (symbols). The solid curve depicts the phase shifts of Eq. (52) with parameters E_b , c , d and f obtained by the fit with this selection of eigenstates; stars and the dashed curve depict the phase shift analysis of experimental data of Refs. [47] and the fit by Eq. (52).

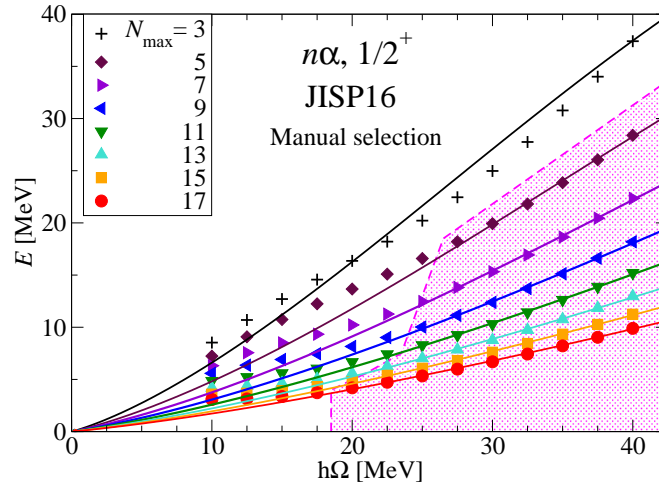


Figure 57: Manual selection the lowest ${}^5\text{He } 1/2^+$ eigenstates E_0 . See Fig. 18 for details.

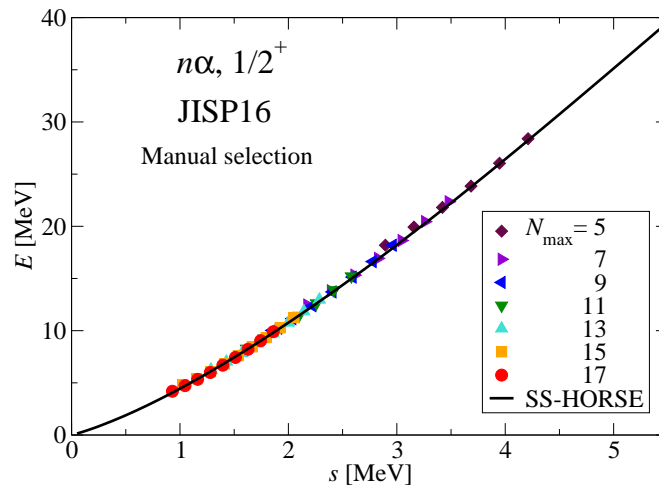


Figure 58: Manually selected ${}^5\text{He } 1/2^+$ eigenstates E_0 plotted as a function of the scaling parameter s (symbols). See Fig. 21 for details.

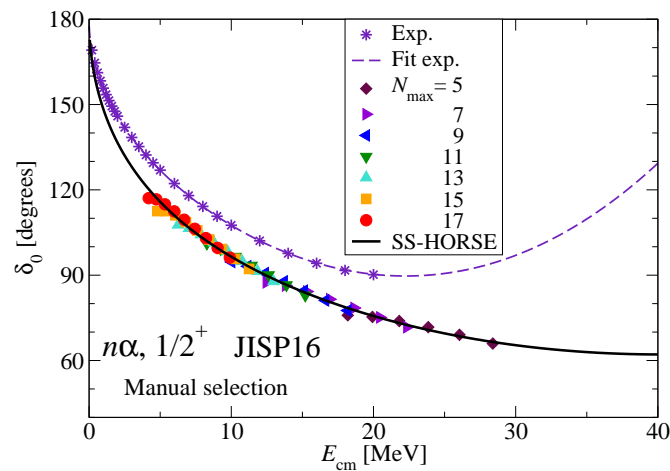


Figure 59: The $1/2^+$ $n\alpha$ phase shifts generated by the manually selected ${}^5\text{He}$ eigenstates E_0 . See Fig. 56 for details.

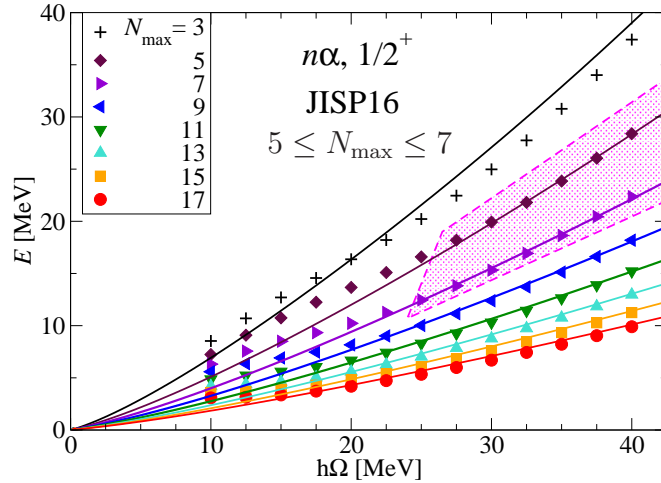


Figure 60: Selection of the lowest ${}^5\text{He } \frac{1}{2}^+$ eigenstates E_0 obtained in NCSM with $5 \leq N_{\text{max}} \leq 7$. See Fig. 18 for details.

It is interesting and important to examine the possibility of describing the eigenenergies and non-resonant phase shifts obtained in many-body calculations in large basis spaces by SS-HORSE fits based on results in much smaller basis spaces. As in the case of $\frac{1}{2}^-$ states, we do not succeed by choosing the eigenstates from the smallest available NCSM basis spaces with $N_{\text{max}} = 3$ and 5: note, in both cases the results from the smallest basis space with $N_{\text{max}} = 2$ for $\frac{1}{2}^-$ and $N_{\text{max}} = 3$ for $\frac{1}{2}^+$ states are not included in our respective manual selections. However picking up eigenstates obtained with $5 \leq N_{\text{max}} \leq 7$ from the manual selection of the ${}^5\text{He } \frac{1}{2}^+$ eigenstates, we obtain reasonable phase shifts and ‘predictions’ for the eigenstates with larger N_{max} , see Figs. 60, 61 and 62. It is interesting that we get similar phase shifts with three different selections of the $\frac{1}{2}^+$ eigenstates while the respective fitting parameters shown in Table 6 differ essentially. The rms deviation of all 53 manually selected $\frac{1}{2}^+$ eigenstates resulting from the fit to 13 eigenstates from the $5 \leq N_{\text{max}} \leq 7$ selection is 259 keV

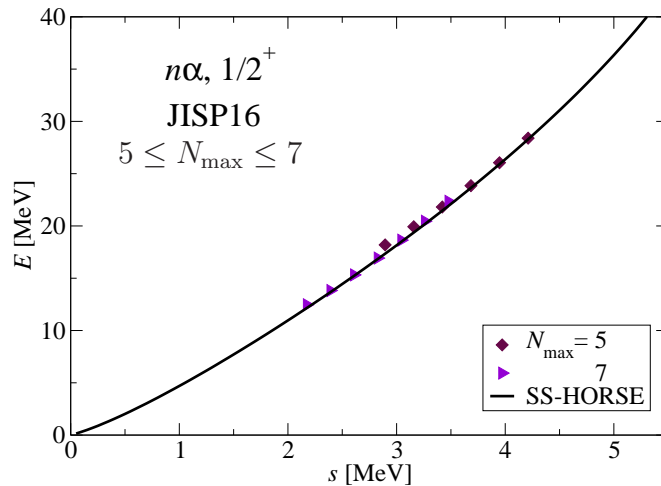


Figure 61: Selected lowest ${}^5\text{He } \frac{1}{2}^+$ eigenstates E_0 obtained in NCSM with $5 \leq N_{\text{max}} \leq 7$ as a function of the scaling parameter s . See Fig. 21 for details.

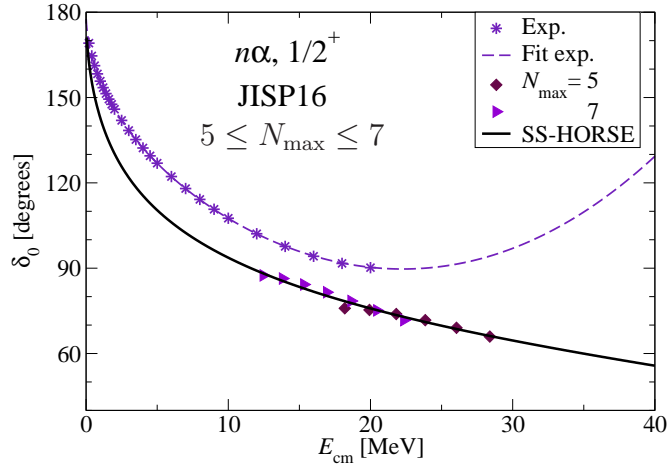


Figure 62: The $\frac{1}{2}^+$ $n\alpha$ phase shifts generated by the selected ${}^5\text{He}$ eigenstates E_0 obtained in NCSM with $5 \leq N_{\max} \leq 7$. See Fig. 56 for details.

that is much worse than the ‘predictions’ of the odd parity eigenstates. We suppose that this is related to the fact that the $\frac{1}{2}^+$ eigenstates lie higher in energy than the $\frac{3}{2}^-$ and $\frac{1}{2}^-$ eigenstates and the SS-HORSE fits, especially those to the small- N_{\max} eigenstates, involve the phase shifts at higher energies where our low-energy phase shift expansions become less accurate and require higher order terms in Taylor series and more fitting parameters.

5 Conclusions

We develop a SS-HORSE approach allowing us to obtain low-energy scattering phase shifts and resonance energy and width in variational calculations with the oscillator basis, in the nuclear shell model in particular. The SS-HORSE technique is based on the general properties of the oscillator basis and on the HORSE (J -matrix) formalism in scattering theory, it utilizes general low-energy expansions of the S -matrix including the poles associated with the bound and resonant states.

The SS-HORSE approach is carefully verified using a model two-body problem with a Woods–Saxon type potential and is shown to be able to obtain accurate scattering phase shifts and resonance energy and width even with small oscillator bases. Next the SS-HORSE method is successfully applied to the study of the $n\alpha$ scattering phases and resonance based on the NCSM calculations of ${}^5\text{He}$ with the realistic JISP16 NN interaction.

Within the SS-HORSE approach we obtain and generalize to the states lying above nuclear disintegration thresholds the scaling property of variational calculations with oscillator basis suggested in Refs. [2, 3] which states that the eigenenergies do not depend separately on $\hbar\Omega$ and the maximal oscillator quanta \mathbb{N} of the states included in the basis but only on their combination s (or the scaling parameter λ_{sc} as suggested in Refs. [2, 3], $s \sim \lambda_{sc}^2$). We demonstrate a typical behavior of eigenstates in the continuum as functions of s in cases when the system has or does not have a low-energy resonance. The scaling property is useful for extrapolating the results obtained in smaller basis spaces to larger bases, and we demonstrate using both the model problem and many-body NCSM calculations that we are able to ‘predict’ accurately the eigenenergies obtained in large bases using the results from much smaller calculations.

We anticipate that the suggested SS-HORSE method will be useful in numerous shell model studies of low-energy nuclear resonances.

We plan to extend the SS-HORSE approach to the case of scattering of charged particles in future publications. We intend also to examine an application of the SS-HORSE method to the study of S -matrix poles corresponding to bound states and to develop the SS-HORSE extrapolation of the variational bound state energies to the infinite basis space.

Acknowledgements

We are thankful to L. D. Blokhintsev and Pieter Maris for valuable discussions. This work was supported in part by the Russian Foundation for Basic Research under Grant No. 15-02-06604-a and by the U.S. Department of Energy under grants No. DESC0008485 (SciDAC/NUCLEI) and DE-FG02-87ER40371. Computational resources were provided by the National Energy Research Scientific Computing Center (NERSC) which is supported by the U.S. Department of Energy under Contract No. DE-AC02-05CH11231.

References

- [1] P. Maris, J. P. Vary and A. M. Shirokov, *Phys. Rev. C* **79**, 014308 (2009).
- [2] S. A. Coon, M. I. Avetian, M. K. G. Kruse, U. van Kolck, P. Maris and J. P. Vary, *Phys. Rev. C* **86**, 054002 (2012).
- [3] S. A. Coon, in *Proc. Int. Workshop Nucl. Theor. Supercomputing Era (NTSE-2012), Khabarovsk, Russia, June 18–22, 2012*, eds. A. M. Shirokov and A. I. Mazur. Pacific National University, Khabarovsk, 2013, p. 171, http://www.ntse-2012.khb.ru/Proc/S_Coon.pdf.
- [4] R. J. Furnstahl, G. Hagen and T. Papenbrock, *Phys. Rev. C* **86**, 031301 (2012).
- [5] S. N. More, A. Ekström, R. J. Furnstahl, G. Hagen and T. Papenbrock, *Phys. Rev. C* **87**, 044326 (2013).
- [6] S. A. Coon and M. K. G. Kruse, in *Proc. Int. Conf. Nucl. Theor. Supercomputing Era (NTSE-2013), Ames, IA, USA, May 13–17, 2013*, eds. A. M. Shirokov and A. I. Mazur. Pacific National University, Khabarovsk, 2014, p. 314, <http://www.ntse-2013.khb.ru/Proc/Coon.pdf>.
- [7] M. K. G. Kruse, E. D. Jurgenson, P. Navrátil, B. R. Barrett and W. E. Ormand, *Phys. Rev. C* **87**, 044301 (2013).
- [8] D. Sääf and C. Forssén, *Phys. Rev. C* **89**, 011303(R) (2014).
- [9] R. J. Furnstahl, S. N. More and T. Papenbrock, *Phys. Rev. C* **89**, 044301 (2014).
- [10] S. König, S. K. Bogner, R. J. Furnstahl, S. N. More and T. Papenbrock, *Phys. Rev. C* **90**, 064007 (2014).
- [11] R. J. Furnstahl, G. Hagen, T. Papenbrock and K. A. Wendt, *J. Phys. G* **42**, 034032 (2015).
- [12] K. A. Wendt, C. Forssén, T. Papenbrock and D. Sääf, *Phys. Rev. C* **91**, 061301(R) (2015).
- [13] S. A. Coon and M. K. G. Kruse, *Int. J. Mod. Phys. E* **25**, 1641011 (2016).

- [14] A. M. Shirokov, A. I. Mazur, J. P. Vary and E. A. Mazur, Phys. Rev. C **79**, 014610 (2009).
- [15] A. M. Shirokov, A. I. Mazur, E. A. Mazur and J. P. Vary, Appl. Math. Inf. Sci. **3**, 245 (2009).
- [16] J. Rotureau, in *Proc. Int. Conf. Nucl. Theor. Supercomputing Era (NTSE-2013), Ames, IA, USA, May 13–17, 2013*, eds. A. M. Shirokov and A. I. Mazur. Pacific National University, Khabarovsk, 2014, p. 236, <http://www.ntse-2013.khb.ru/Proc/Rotureau.pdf>.
- [17] G. Papadimitriou, J. Rotureau, N. Michel, M. Płoszajczak and B. R. Barrett, Phys. Rev. C **88**, 044318 (2013).
- [18] P. Navrátil, S. Quaglioni, I. Stetcu and B. R. Barrett, J. Phys. G **36**, 083101 (2009).
- [19] P. Navrátil, in *Proc. Int. Conf. Nucl. Theor. Supercomputing Era (NTSE-2013), Ames, IA, USA, May 13–17, 2013*, eds. A. M. Shirokov and A. I. Mazur. Pacific National University, Khabarovsk, 2014, p. 211, <http://www.ntse-2013.khb.ru/Proc/Navratil.pdf>.
- [20] G. Hupin, J. Langhammer, P. Navrátil, S. Quaglioni, A. Calci and R. Roth, Phys. Rev. C **88**, 054622 (2013).
- [21] S. Quaglioni, P. Navrátil, G. Hupin, J. Langhammer, C. Romero-Redondo and R. Roth, Few-body Syst. **54**, 877 (2013).
- [22] B. R. Barrett, P. Navrátil and J. P. Vary, Progr. Part. Nucl. Phys **69**, 131 (2013).
- [23] G. Hupin, S. Quaglioni and P. Navrátil, Phys. Rev. C **90**, 061601(R) (2014).
- [24] E. J. Heller and H. A. Yamany, Phys. Rev. A **9**, 1201 (1974); *ibid.* 1209 (1974).
- [25] H. A. Yamany and L. Fishman. J. Math. Phys. **16**, 410 (1975).
- [26] G. F. Filippov and I. P. Okhrimenko, Yad. Fiz. **32**, 932 (1980) [Sov. J. Nucl. Phys. **32**, 480 (1980)]; G. F. Filippov, Yad. Fiz. **33**, 928 (1981) [Sov. J. Nucl. Phys. **33**, 488 (1981)].
- [27] Yu. F. Smirnov and Yu. I. Nechaev, Kinam **4**, 445 (1982); Yu. I. Nechaev and Yu. F. Smirnov, Yad. Fiz. **35**, 1385 (1982) [Sov. J. Nucl. Phys. **35**, 808 (1982)].
- [28] V. A. Knyr, A. I. Mazur and Yu. F. Smirnov, Yad. Fiz. **52**, 754 (1990) [Sov. J. Nucl. Phys. **52**, 483 (1990)]; Yad. Fiz. **54**, 1518 (1991) [Sov. J. Nucl. Phys. **54**, 927 (1991)]; Yad. Fiz. **56**(10), 72 (1993) [Phys. At. Nucl. **56**, 1342 (1993)]; A. I. Mazur and S. A. Zaytsev, Yad. Fiz. **62**, 656 (1999) [Phys. At. Nucl. **62**, 608 (1999)].
- [29] J. M. Bang, A. I. Mazur, A. M. Shirokov, Yu. F. Smirnov and S. A. Zaytsev, Ann. Phys. (NY) **280**, 299 (2000).
- [30] V. I. Kukulin, V. N. Pomerantsev and O. A. Rubtsova, JETP Lett. **90**, 402 (2009); O. A. Rubtsova, V. I. Kukulin, V. N. Pomerantsev and A. Faessler, Phys. Rev. C **81**, 064003 (2010).
- [31] I. M. Lifshitz, Zh. Eksp. Teor. Fiz. **17**, 1017 (1947) (*in Russian*); *ibid.* **17**, 1076 (1947) (*in Russian*); Usp. Mat. Nauk **7**, 171 (1952) (*in Russian*).
- [32] T. Luu, M. J. Savage, A. Schwenk and J. P. Vary, Phys. Rev. C **82**, 034003 (2010).

- [33] R. M. Nollett, Phys. Rev. C **86**, 044330 (2012).
- [34] A. M. Shirokov, J. P. Vary, A. I. Mazur and T. A. Weber, Phys. Lett. B **644**, 33 (2007).
- [35] A Fortran code generating the JISP16 matrix elements is available at <http://nuclear.physics.iastate.edu>.
- [36] I. A. Mazur, A. M. Shirokov, A. I. Mazur and J. P. Vary, arXiv:1512.03983 [nucl-th] (2015).
- [37] A. M. Shirokov, A. I. Mazur, I. A. Mazur and J. P. Vary, arXiv:1608.05885 [nucl-th] (2016).
- [38] A. I. Mazur, A. M. Shirokov, J. P. Vary, P. Maris and I. A. Mazur, in *Proc. Int. Workshop Nucl. Theor. Supercomputing Era (NTSE-2012), Khabarovsk, Russia, June 18–22, 2012*, eds. A. M. Shirokov and A. I. Mazur. Pacific National University, Khabarovsk, 2013, p. 146, http://www.ntse-2012.khb.ru/Proc/A_Mazur.pdf.
- [39] A. D. Alhaidari, E. J. Heller, H. A. Yamani and M. S. Abdelmonem (eds.), *The J-matrix method. Developments and applications*. Springer, 2008.
- [40] A. M. Shirokov, Yu. F. Smirnov and S. A. Zaytsev, in *Modern problems in quantum theory*, eds. V. I. Savrin and O. A. Khrustalev. Moscow, 1998, p. 184; S. A. Zaytsev, Yu. F. Smirnov and A. M. Shirokov, Teoret. Mat. Fiz. **117**, 227 (1998) [Theor. Math. Phys. **117**, 1291 (1998)].
- [41] A. M. Shirokov, A. I. Mazur, S. A. Zaytsev, J. P. Vary and T. A. Weber, Phys. Rev. C **70**, 044005 (2004); in *The J-matrix method. Developments and applications*, eds. A. D. Alhaidari, E. J. Heller, H. A. Yamani and M. S. Abdelmonem. Springer, 2008, p. 219.
- [42] A. I. Baz', Ya. B. Zel'dovich and A. M. Perelomov, *Scattering, reactions and decay in non-relativistic quantum mechanics*. Israel Program for Scientific Translation, Jerusalem, 1969.
- [43] R. G. Newton, *Scattering theory of waves and particles, 2nd. ed.* Springer-Verlag, New York, 1982.
- [44] J. Bang and C. Gignoux, Nucl. Phys. A **313**, 119 (1979).
- [45] P. Maris, M. Sosonkina, J. P. Vary, E. G. Ng and C. Yang, Proc. Comput. Sci. **1**, 97 (2010).
- [46] H. M. Aktulga, C. Yang, E. G. Ng, P. Maris and J. P. Vary, Concurrency Computat. Pract. Exper. **26**, 2631 (2014).
- [47] J. E. Bond and F. W. K. Firk, Nucl. Phys. A **287**, 317 (1977).
- [48] A. Csóto and G. M. Hale, Phys. Rev. C **55**, 536 (1997).
- [49] A. M. Shirokov, G. Papadimitriou, A. I. Mazur, I. A. Mazur, R. Roth and J. P. Vary, arXiv:1607.05631 [nucl-th] (2016).
- [50] A. M. Shirokov, G. Papadimitriou, A. I. Mazur, I. A. Mazur, R. Roth and J. P. Vary, *see these Proceedings*, p. 174, <http://www.ntse-2014.khb.ru/Proc/Shirokov.pdf>.